General Spectral Computations of the Nonlinear Shallow Water Tidal Interactions within the Bight of Abaco

J. J. WESTERINK

Ocean Engineering Program, Civil Engineering Department, Texas A&M University, College Station, Texas

K. D. STOLZENBACH AND J. J. CONNOR

Department of Civil Engineering, Massachusetts Institute of Technology, Cambridge, Massachusetts

(Manuscript received 15 July 1988, in final form 23 February 1989)

ABSTRACT

An iterative frequency–time domain finite element tidal circulation model is applied to the Bight of Abaco in the Bahamas to study the nonlinear interactions that occur between the various astronomical, overtide and compound-tide constituents. The nonlinear origin of the significant shallow water constituents is determined by suppressing the various nonlinear terms in the shallow water equations. Furthermore, the extent to which nonlinear constituents interact with and affect each other is studied in detail by suppressing the interaction of selected tides within the framework of the iterative frequency–time domain formulation. It is found that secondary nonlinear interactions between the astronomical tides and the shallow water tides themselves can significantly affect overtides, compound tides and even astronomical tides. Some important examples include (i) the M_2 interaction with M_6 which generates the M_8 tide, (ii) the significant reductions in M_6, M_8 and M_{10} responses (respectively by 12%, 15% and 25%) due to the interaction involving the $2MN_2$ and $2MS_2$ constituents, and (iii) increased responses in the N_2 and S_2 constituents (by about 7%) due to interactions with the $2MN_2$ and $2MS_2$ tides.

1. Introduction

Interest in developing an increasingly more accurate predictive capability of sea level elevation and circulation in the coastal zone has been spurred on by concerns relating to navigation, shoreline flooding and pollutant transport. Typically, site specific sea level data is based on the harmonic analysis of a measured time history signal which yields harmonic tidal constituents which are then used to regenerate time history signals at future times. More recently numerical models have come into use as predictive tools which are able to provide more global information.

Harmonic tidal constituents have associated frequencies which relate to the forcings which generate them and their use has a firm mathematical and historical basis. They are broadly classified as either astronomical constituents, which are generated through gravitational attraction of the moon and sun, or shallow water constituents, which are the result of the interactions of the astronomical constituents with each other or with other shallow water constituents through the nonlinear processes which govern the flow in the waterbody. The shallow water constituents gain significance in shallow coastal areas, and in order to accurately represent the surface profile and circulation in these regions it is absolutely essential that these constituents be concisely computed.

It has been a matter of long standing interest as to which nonlinear mechanisms generate the shallow water tides and, furthermore, how these constituents mutually interact and modify each other (Dronkers 1964). A number of recent studies have given considerable insight into these questions and have in particular paid much deserved attention to the nonlinear friction terms (LeBlond 1978; Kabbaj and Le Provost 1980; Le Provost and Fornerino 1985; Parker 1986; Walters and Werner 1988). The present study, through a numerical investigation of the tides in the shallow Bight of Abaco in the Bahamas, examines in detail the extent to which the various nonlinearities generate the shallow water constituents in addition to the degree to which the various nonlinear constituents affect each other. We will focus in particular on the details of the secondary nonlinear interactions which occur between the astronomical constituents and/or the shallow water constituents.

The numerical model used in this study, TEA-NL (Nonlinear Tidal Embayment Analysis), allows for the entirely general investigation of these nonlinear tidal interactions. TEA-NL is a harmonic finite element tidal prediction model, which solves for the full nonlinear

Corresponding author address: Dr. Joannes J. Westerink, Ocean Engineering Program, Civil Engineering Department, Texas A&M University, College Station, TX 77843.

form of the shallow water equations (Westerink et al. 1987, 1988). Harmonic tidal models have come into recent use due to a number of potential advantages over time stepping models in addition to allowing for the direct computation of tidal constituents (Kawahara et al. 1977; Pearson and Winter 1977; Le Provost and Poncet 1978; Snyder et al. 1979; Le Provost et al. 1981; Walters 1986, 1988; Lynch and Werner 1987). Model TEA-NL embodies a variety of unique features which make it entirely general with respect to being able to selectively examine tidal constituents of any type (astronomical, overtide and compound tide) and to fully control the associated nonlinear interactions. These capabilities result from the use of an iterative frequency–time domain formulation in conjunction with the least squares harmonic analysis method.

The study area used for our investigation, the Bight of Abaco, is ideally suited for our purposes. The shallow water depths (1 to 9 m) within the embayment cause an extensive number of shallow water constituents to be generated. Furthermore, the very large open ocean depths outside of the bight (1000 to 2000 m) not only assure that any shallow water species within the bight are generated there but also significantly simplifies the setting of the shallow water constituent boundary conditions to zero due to the almost fully out-of-phase reflective behavior of the open ocean boundary. Thus the topography and location of the Bight of Abaco allow the generation and interaction of the shallow water constituents to be precisely and conveniently examined. In addition, a comprehensive field investigation carried out by Filloux and Snyder (1979) has produced extensive tidal data at 25 locations within the bight for five major astronomical constituents (M_2, N_2, S_2, O_1 and K_1) and two major overtide constituents (M_4 and M_6). Finally, previous numerical studies of the bight (Snyder et al. 1979) overpredicted the M_6 constituent by roughly a factor of two and thus posed some very interesting questions regarding the validity of the standard quadratic bottom friction law or the possibility of other significant dissipative mechanisms existing at this site.

Our model application to the Bight of Abaco systematically examines how the nonlinearities generate the shallow water constituents and to what extent these constituents interact with each other by selectively suppressing the interaction of certain overtide and compound constituents. This not only provides considerable insight into nonlinear shallow water dynamics but in doing so also demonstrates the versatility and power of harmonic numerical models.

2. Description of the numerical model TEA-NL

a. Governing equations

Model TEA-NL solves for the well-known shallow water equations. These equations express continuity and conservation of momentum integrated over depth and are written as

$$\eta_{,t} + [u(h+\eta)]_{,x} + [v(h+\eta)]_{,y} = 0 \tag{1}$$

$$u_{,t} + g\eta_{,x} - fv + c_f \frac{(u^2+v^2)^{1/2}}{(h+\eta)} u + (uu_{,x} + vu_{,y}) = 0 \tag{2a}$$

$$v_{,t} + g\eta_{,y} + fu + c_f \frac{(u^2+v^2)^{1/2}}{(h+\eta)} v + (uv_{,x} + vv_{,y}) = 0 \tag{2b}$$

where

t	time
x, y	cartesian coordinates
u, v	depth averaged components of velocity
η	surface elevation relative to undisturbed sea surface level
h	depth of undisturbed sea surface level
g	acceleration due to gravity
f	Coriolis factor
c_f	bottom friction coefficient.

The nonlinearities are of particular interest since they cause the coupling and interaction between the tides in shallow water. These nonlinearities consist of (i) a finite amplitude component of flux terms in the continuity equation, (ii) quadratic friction terms which also include a finite amplitude component in the momentum equation, and (iii) the convective acceleration terms in the momentum equations. Since the nonlinear terms will be handled in an iterative fashion, they are all moved to the right-hand side of the equations. A linear friction term is now added to both sides of the momentum equations to provide iterative stability and improve convergence rates. Thus the governing equations now appear as

$$\eta_{,t} + (uh)_{,x} + (vh)_{,y} = -(u\eta)_{,x} - (v\eta)_{,y} \tag{3}$$

$$u_{,t} + g\eta_{,x} - fv + \lambda u = \left[\lambda - c_f \frac{(u^2+v^2)^{1/2}}{(h+\eta)}\right] u - (uu_{,x} + vu_{,y}) \tag{4a}$$

$$v_{,t} + g\eta_{,y} + fu + \lambda v = \left[\lambda - c_f \frac{(u^2+v^2)^{1/2}}{(h+\eta)}\right] v - (uv_{,x} + vv_{,y}) \tag{4b}$$

where λ = linearized friction factor.

Corresponding to the governing equations are a set of boundary conditions consisting of the prescription of elevation, η^*, on open ocean boundaries and the prescription of normal flux, Q_n^*, on land and river boundaries. These boundary conditions are respectively expressed as

$$\eta = \eta^* \quad \text{on } \Gamma_\eta \tag{5a}$$

$$Q_n = Q_n^* \quad \text{on } \Gamma_Q. \tag{5b}$$

Since we will be reducing the governing equation to sets of quasi-steady harmonic equations, no initial conditions are required.

b. Numerical formulation

A Galerkin finite element procedure is used to resolve the spatial dependence of the governing equations. However, standard Galerkin methods typically result in solutions with severe spurious oscillations with wavelengths on the order of twice the grid size. Our formulation tackles this problem by relaxing the treatment of the flux prescribed boundary conditions such that they are handled as natural boundary conditions in the weighted residual formulation. Applications of our formulation to stringent two-dimensional test problems have shown that this formulation results in very good solutions exhibiting low spurious oscillations without introducing numerical damping (Westerink et al. 1987, 1988).

Developing our Galerkin weighted residual formulation and applying the finite element method with C^0 interpolation results in the following system of differentially time dependent algebraic equations:

$$\mathbf{M}_\eta \eta_{,t} - \mathbf{D}\mathbf{U} = -\mathbf{P}_\eta^{\text{lin}} + \mathbf{P}_\eta^{\text{nl}} \tag{6}$$

$$\mathbf{M}_U \mathbf{U}_{,t} + \mathbf{M}_F \mathbf{U} + \mathbf{M}_C \mathbf{U} + g\mathbf{D}^T \eta = \mathbf{P}_{\Delta-\text{fric}}^{\text{nl}} - \mathbf{P}_{\text{conv}}^{\text{nl}}, \tag{7}$$

where

- η vector of nodal elevation values
- $\mathbf{U}$ vector of nodal velocity values (x and y components)
- $\mathbf{M}_\eta$ continuity equation coefficient matrix
- $\mathbf{M}_U$ momentum equation mass matrix
- $\mathbf{M}_F$ linearized friction distribution matrix
- $\mathbf{M}_C$ Coriolis matrix
- $\mathbf{P}_\eta^{\text{lin}}$ load vector for flux prescribed boundaries
- $\mathbf{P}_\eta^{\text{nl}}$ nonlinear load vector for continuity equation finite amplitude effects
- $\mathbf{P}_{\Delta-\text{fric}}^{\text{nl}}$ nonlinear load vector containing the difference between linearized friction and full nonlinear friction terms, and
- $\mathbf{P}_{\text{conv}}^{\text{nl}}$ nonlinear load vector for convective acceleration effects.

TEA-NL has been implemented with equal order linear interpolation over triangular elements for elevation, velocity, depths and friction factors (Westerink et al. 1987, 1988).

To resolve the time dependence in (6) and (7) we assume that response as well as linear and nonlinear load vectors may be expressed as harmonic series of the form:

$$\mathbf{A}(t) = \text{Re}\{\sum_{j=1}^{N_f} \hat{\mathbf{A}}_j e^{i\omega_j t}\}, \tag{8}$$

where

- $\mathbf{A}(t)$ representative vector for the time history of the responses η and $\mathbf{U}$ and any of the load vectors
- $\hat{\mathbf{A}}_j$ complex amplitude of the jth harmonic constituent of $\mathbf{A}(t)$—both magnitude and phase shift are represented
- i $(-1)^{1/2}$
- ω_j jth frequency of the spectrum, and
- N_f number of frequencies required to adequately represent the significant constituents of the tidal spectrum.

Substituting the harmonic series representation for the responses and load vectors into (6) and (7) leads to $j = 1, N_f$ sets of time independent systems of equations of the form:

$$i\omega_j \mathbf{M}_\eta \hat{\eta}_j - \mathbf{D}\hat{\mathbf{U}}_j = -\hat{\mathbf{P}}_{\eta_j}^{\text{lin}} + \hat{\mathbf{P}}_{\eta_j}^{\text{nl}} \tag{9}$$

$$i\omega_j \mathbf{M}_U \hat{\mathbf{U}}_j + \mathbf{M}_F \hat{\mathbf{U}}_j + \mathbf{M}_C \hat{\mathbf{U}}_j + g\mathbf{D}^T \hat{\eta}_j = \hat{\mathbf{P}}_{\Delta-\text{fric}_j}^{\text{nl}} - \hat{\mathbf{P}}_{\text{conv}_j}^{\text{nl}}. \tag{10}$$

Each system of equations is coupled to the other ($N_f - 1$) systems of equations through the right-hand side nonlinear load vectors. This nonlinear coupling between harmonics is handled using an iterative solution strategy which iteratively updates these right-hand side load vectors and thus linearizes each system of equations at each cycle of the iteration.

The iterative solution starts with the assumption that all the harmonic right-hand side nonlinear load vectors are equal to zero. Harmonic responses in elevation and velocity are then computed by solving (9) and (10) for N_b frequencies with nonzero boundary forcings. Time histories of elevation and velocity responses, $\eta(t)$ and $U(t)$, are now generated using (8) and the computed harmonic response amplitudes, $\hat{\eta}_j$ and $\hat{U}_j$, $j = 1, N_b$. Next, time histories for each of the nonlinear load vectors, $\mathbf{P}_\eta^{nl}(t)$, $\mathbf{P}_{\Delta-\text{fric}}^{\text{nl}}(t)$ and $\mathbf{P}_{\text{conv}}^{\text{nl}}(t)$, are generated using the response time histories. These nonlinear load time histories are now spectrally decomposed, using the least squares harmonic analysis procedure, into harmonic nonlinear load vectors, $\hat{\mathbf{P}}_{\eta_j}^{\text{nl}}$, $\hat{\mathbf{P}}_{\Delta-\text{fric}_j}^{\text{nl}}$ and $\hat{\mathbf{P}}_{\text{conv}_j}^{\text{nl}}$, for a set of N_f significant frequencies. Now responses are computed for frequencies with nonzero boundary forcings in addition to frequencies with significant harmonic nonlinear forcings by solving (9) and (10) for this larger set of frequencies. The procedure is now repeated by again updating the time and harmonic load vectors and recomputing responses until a specified threshold of convergence is achieved (Westerink et al. 1987, 1988).

To improve convergence rates and ensure iterative stability we included a linearized friction factor on both sides of the momentum equations. This linearized friction factor is locally optimized prior to starting the

nonlinear iteration just described. This optimization is based on the assumption that a dominant tide such as the M_2 exists and is implemented by iteratively computing linear responses for the dominant tide alone and then updating local λ values using the specified values of c_f, the updated local velocity amplitude of the dominant tide, in addition to a coefficient found by Fourier expanding the nonlinear friction term. Typically after about five of these linear cycles, λ values have converged sufficiently. These final values of λ are then relaxed by multiplying them by a factor of 1.5 (Westerink et al. 1988).

c. *Least squares harmonic analysis method*

We have selected the least squares (LSQ) harmonic analysis method in order to harmonically decompose the time histories of the nonlinear load vectors in our iterative solution. This procedure simply consists of a standard least squares error minimization process which uses a harmonic series as the fitting function. A LSQ matrix results which must be solved.

The LSQ method is ideally suited for the analysis of tidal data since it is highly frequency selective and the number of required time history sampling points is theoretically related only to the number of frequencies in the spectrum and not the frequency resolution. These features make the LSQ method very attractive for tidal data analysis since tidal records have very irregular frequency distributions consisting of widely spaced clusters within which harmonics are very closely spaced (Horn 1959; Van Ette and Schoemaker 1967; Godin 1970).

The LSQ method is commonly used to harmonically analyze field measured tidal elevation records. The method is even better qualified for the harmonic analysis of our analytically generated nonlinear load vectors for a variety of reasons. First of all, these analytically generated signals do not include any nontidal noise and the frequency content is precisely known. Second, the time sampling point distribution can be precisely and conveniently controlled such that errors associated with computer roundoff due to a possible ill-conditioned LSQ matrix and errors associated with the necessary truncation of the harmonic sampling series are minimized. These errors are controlled by adjusting the degree of diagonal dominance of a set of LSQ matrices. The time sampling spacing and time history record length which yield low LSQ analysis errors are very specific to the frequency content of the signal being analyzed and are typically both very large. Thus while the required time history record length is very large, the actual number of time sampling points remains very modest due to the associated large time sampling step. Therefore this tailoring of the LSQ method allows for very accurate yet extremely economical LSQ analyses to be performed for the analytically generated nonlinear loading signals (Westerink et al. 1988).

3. Description of the Bight of Abaco

a. *Physical characteristics*

The Bight of Abaco, shown in Fig. 1, is a shallow embayment with land boundaries consisting of the Island of Abaco along the southern and eastern boundaries and the island of Little Abaco and Grand Bahama along the northern boundary. The western boundary is predominantly connected to the open ocean. The bight is roughly 100 km in length and 40 km in width.

The bathymetry within the bight is shown in Fig. 2. In the region along the open ocean boundary depths vary between 2 and 5 meters. This region actually forms a sill since depths increase again in the interior of the bight. In the northern half of the bight a depression with depths between 7 and 8 meters exists. Depths become extremely shallow along the northern boundary. Outside of the bight depths drop very rapidly. In fact, the 200-m contour lies between 1 to 3 km seaward of the sill region and depths drop to more than 1000 meters within 3 to 15 km from the sill.

Bottom characteristics also vary somewhat within the bight. The sill region has a bottom surface characterized by numerous sand waves with heights between 1 and 3 m. These sand bores are not represented in the depth distribution. The northern depression region contains muddy mounds with heights of 10 cm and a horizontal scale of several meters. The relatively flat southern portion of the bight has a bottom surface consisting of thin sediment cover over rock, punctuated

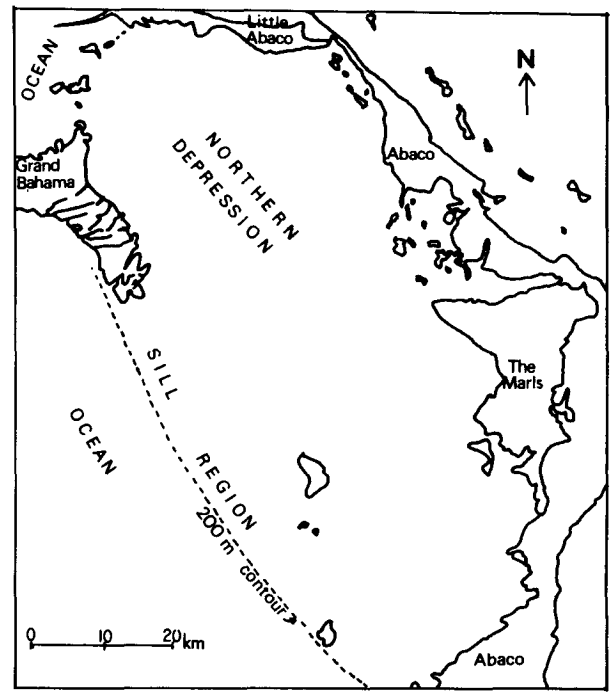

FIG. 1. Bight of Abaco, Bahamas.

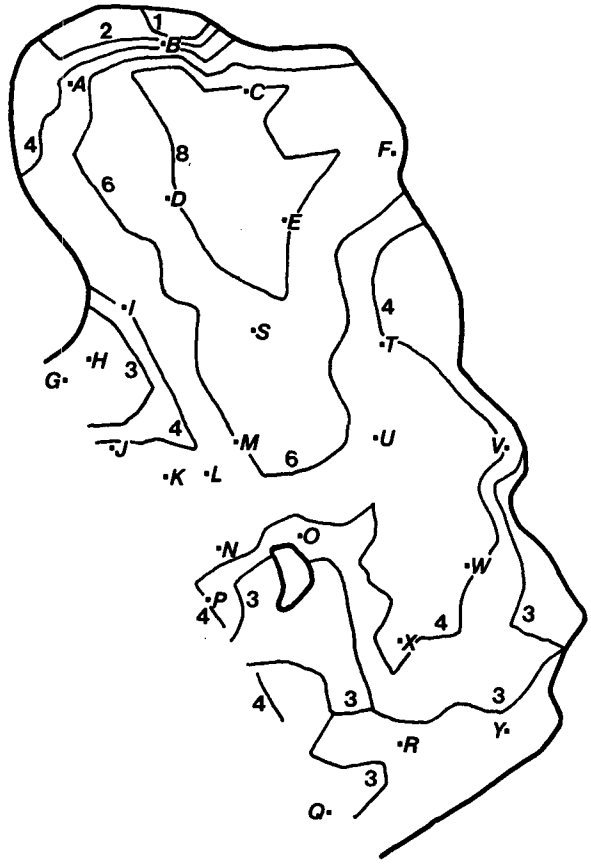

FIG. 2. Bathymetry of the Bight of Abaco in meters with field data measurement locations indicated.

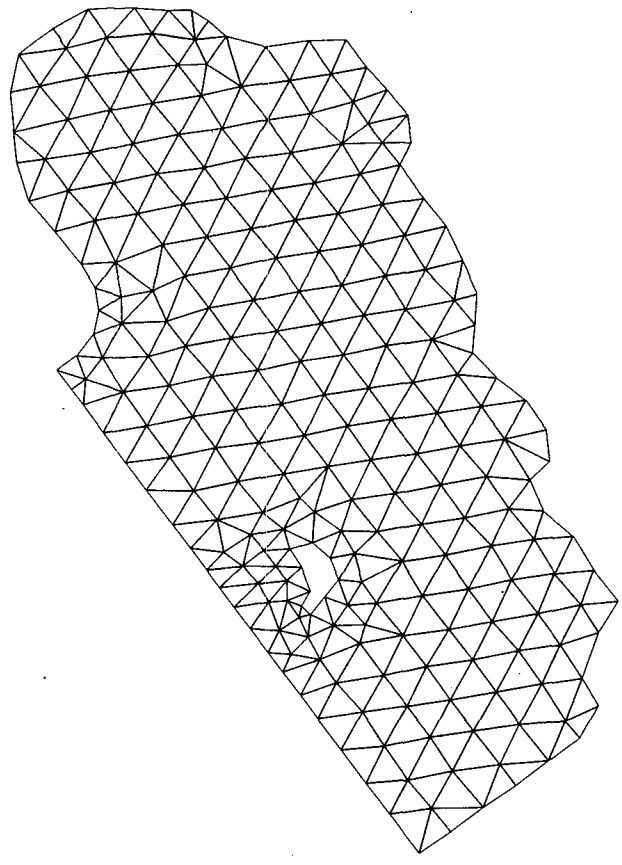

FIG. 3. Finite element discretization of the Bight of Abaco.

in patches by sea fans and corals (Filloux and Snyder 1979; Snyder et al. 1979).

b. *Computational grid and boundary conditions*

The finite element discretization for the Bight of Abaco is shown in Fig. 3. The open ocean boundary for the grid corresponds to the outer sill where the very sharp depth gradient begins.

Detailed tidal forcing information must be specified on the open ocean boundary. Field data collected by Filloux and Snyder (1979) is used in the specification of the incoming astronomical constituents on this boundary. Boundary forcing data for the five main astronomical constituents is shown in Table 1. Each constituent is essentially constant along the entire open ocean boundary.

The specification of nonlinear shallow water constituents is also quite straightforward. As the nonlinear tides generated within the bight reach the open ocean boundary, they are largely reflected, out of phase, back into the bight. For a long wave passing over a step with a shallow to deep water depth ratio of the bight, varying between 0.005 and 0.001, the computed reflection coefficient varies between −0.87 and −0.94 (Ippen 1966). Thus it is a reasonable approximation to assume that these nonlinear waves are fully reflected. In conjunction with the fact that no significant nonlinear tidal species exist in the open ocean, we can conveniently specify all nonlinear shallow water tides equal to zero on the open ocean boundary.

All land boundaries are treated as flux prescribed boundary conditions on which normal flux is set to zero. It is noted that a number of very shallow connections in the northwestern part of the bight are also treated as land boundaries. The data taken by Filloux and Snyder (1979) showed that these openings were

TABLE 1. Ocean boundary forcing values for astronomical constituents from measured data.

Tide	Amplitude (cm)	Phase lag (degrees relative to M_2)
O_1	7.5	195
K_1	9.5	207
N_2	10.0	340
M_2	39.5	0
S_2	6.0	43

TABLE 2. List of frequencies used for M_2 overtide cases (Cases O-1 through O-13).

Tide	Frequency (rad sec^{-1})	Period (h)
Steady	0.00000000000	—
M_2	0.00014051892	12.42
M_4	0.00028103783	6.21
M_6	0.00042155675	4.14
M_8	0.00056207567	3.11
M_{10}	0.00070259459	2.48
M_{12}	0.00084311350	2.07
M_{14}	0.00098363242	1.77
M_{16}	0.00112415134	1.55
M_{18}	0.00126467025	1.38

relatively opaque to the tides and therefore could be simply treated as land boundaries.

4. Overtide computations in the Bight of Abaco

We shall first consider a series of cases with the dominant M_2 tide as the only astronomical forcing tide and the M_2 overtides as the only nonlinearly generated shallow water tides. This preliminary approach offers simplicity and clarity in examining a number of different issues including the variability in basin response with changing bottom friction, the extent to which the different nonlinear terms generate the various nonlinear tides and the mutual interaction of these tides.

We shall consider, together with the M_2 forcing tide, the nine M_2 overtide constituents listed in Table 2. The M_2 tide is specified as 39.5 cm along the open ocean and all overtide constituents are specified as zero along this boundary. All ten frequencies were used in the harmonic analysis of the time history loading signals. However, except when noted, only the first six frequencies (steady state–M_{10} constituents) were allowed to backfeed into the signal (i.e., were used in the generation of an updated response time history). The LSQ harmonic analysis was applied using a central time origin with 38 evenly spaced time sampling points distributed exactly over the period of modulation of the signal, 12.42 hours. This leads to LSQ submatrices which are entirely diagonal.

a. Basin response characteristics with varying bottom friction factor

In this subsection we shall determine the influence of varying the bottom friction factor, c_f, on basin responses. All nonlinear terms in the governing equations are included in the computations. It is noted that all damping in the basin results from friction alone since model TEA-NL neither includes user specified eddy viscosity type terms nor introduces numerical damping as a result of the numerical discretization. Table 3 shows the effect of varying c_f on the basin averaged responses in elevation, $\hat{\eta}_j$, and velocity, $\bar{U}_j$, at the various frequencies. These friction factors, which range between 0.003 and 0.012, were used over the entire bight. A decrease in M_2 response is seen as c_f increases. A corresponding decrease is seen in all the basin average overtide responses, with the exception of $\hat{\eta}_j$ at steady state.

It appears that basin average elevation and basin average velocity maintain approximately the same ratio over the range of c_f values at a given frequency with the exception of the steady state constituent. Furthermore, the average elevation to average velocity ratios remain the same to within a factor of approximately two at a given c_f value for all constituents, again with the exception of steady state. Thus basin average ele-

TABLE 3. Basin-averaged harmonic elevation (in meters) and velocity (m s^{-1}) responses for the M_2 astronomical boundary forcing cases with varying friction factor (numbers given to 3 or more significant figures).

			Constituent					
Case	c_f	Variable	Steady	M_2	M_4	M_6	M_8	M_{10}
O-1	0.0030	$\bar{\eta}_j$	0.0202	0.299	0.0148	0.0133	0.00264	0.00640
		$\bar{U}_j$	0.0106	0.222	0.0161	0.0237	0.00422	0.00776
O-2	0.0060	$\bar{\eta}_j$	0.0203	0.239	0.0100	0.0116	0.00214	0.00526
		$\bar{U}_j$	0.00569	0.164	0.0105	0.0188	0.00328	0.00655
O-3	0.0090	$\bar{\eta}_j$	0.0204	0.211	0.00821	0.0107	0.00192	0.00462
		$\bar{U}_j$	0.00422	0.137	0.00836	0.0161	0.00280	0.00575
O-4	0.0095	$\bar{\eta}_j$	0.0204	0.208	0.00802	0.0106	0.00189	0.00454
		$\bar{U}_j$	0.00407	0.134	0.00811	0.0158	0.00274	0.00564
O-5	0.0100	$\bar{\eta}_j$	0.0204	0.205	0.00783	0.0105	0.00187	0.00447
		$\bar{U}_j$	0.00394	0.131	0.00789	0.0155	0.00268	0.00554
O-6	0.0120	$\bar{\eta}_j$	0.0204	0.194	0.00725	0.0101	0.00179	0.00422
		$\bar{U}_j$	0.00350	0.120	0.00714	0.0143	0.00249	0.00519

vation amplitude appears to be an adequate measure of the importance of a constituent except at steady state. Thus we shall use $\bar{\eta}_j$ as the principle basis of comparison of computed tides in this paper, but it must be kept in mind that $\bar{\eta}_j$ will not be a good indication of the relative importance of low frequency constituents.

The increased resolution indicated in Table 3 around $c_f = 0.0095$ is provided since this value corresponds to the optimal friction factor which yields the best agreement between Filloux and Snyder's (1979) measurements and TEA-NL overtide computations for the main M_2 tide. For the M_4 tide this value provides a near minimum error. However, for the M_6 tide there is no apparent local minimum in this c_f range and a discrepancy between measurements and computations of a factor of about two exists at $c_f = 0.0095$. Details of the error analysis are given in section 6.

An optimal friction factor equal to 0.0095 at first seems somewhat high. However, when considering the depths and bottom characteristics of the bight, this factor is well founded. The dunes and shallow depths in the sill region lead to especially high c_f values. For dunes of one meter height, in water depths ranging from 2 to 5 meters, the friction factor ranges between 0.0125 and 0.0092 (using a Manning n equal to 0.040). In the northern depression and southeastern portion of the bight, friction values are somewhat lower and we estimate values equal to approximately 0.003. Therefore it appears that the optimal friction factor is physically well justified in the sill region but not in other portions of the bight. However, the sill region is the most important region in the bight with respect to M_2 damping and nonlinear tide generation due to the fact that the highest velocities, the largest elevations and the shallowest depths in the bight occur in this region. In fact, we found that using lower friction factor values in the northern and southeastern portions of the bight did not significantly alter response computations. This concurs with the findings of Snyder et al. (1979). Thus we shall use friction factors which are constant throughout the domain and in fact, for the bulk of the remaining computations, use the value $c_f = 0.0095$.

b. Nonlinearities and the overtides they generate

In this subsection we shall investigate the origins of both the nonlinear forcings and responses in addition to examining how the shallow water constituents interact through these nonlinearities. The approach we take is to selectively neglect in our computations certain nonlinear terms and to compare the resulting basin averaged harmonic forcings and responses. The cases examined are summarized in Table 4. Basin averaged amplitudes of the harmonic nonlinear finite amplitude forcing components for the continuity equation, $\bar{P}_{\eta_j}$, and the nonlinear friction and convective acceleration components for the momentum equation, $\bar{P}_{U_j}$ (i.e., the nonlinear portion of $\hat{\mathbf{P}}^{\mathrm{nl}}_{\Delta-\mathrm{fric}_j}$ and $\hat{\mathbf{P}}^{\mathrm{nl}}_{\mathrm{conv}_j}$), in addition to basin averaged harmonic responses in elevation, $\bar{\eta}_j$, and velocity, $\bar{U}_j$, are given in Table 5.

TABLE 4. Run sequence for nonlinear overtide interactions—nonlinearity included (yes/no).

Case	Finite amplitude in continuity	Quadratic friction	Finite amplitude in friction term	Convective acceleration
O-7	yes	no	no	no
O-8	no	yes	no	no
O-9	no	yes	yes	no
O-10	yes	yes	no	no
O-11	yes	yes	yes	no
O-4	yes	yes	yes	yes

1) CASE O-7: THE EFFECT OF FINITE AMPLITUDE IN THE CONTINUITY EQUATION

Let us first consider only the effect of the finite amplitude term in the continuity equation. We turn off the nonlinear quadratic friction term and convective acceleration terms such that all momentum equation nonlinear harmonic forcings, $\bar{P}_{U_j}$, are equal to zero. However, linearized friction factors are updated in five purely linear iterations computing only the linear M_2 response as described in section 2b with the exception that no relaxation factor is applied. $\mathbf{P}^{\mathrm{nl}}_{\Delta-\mathrm{fric}}$ is then set to zero at all nodes. It is noted by comparing the M_2 response for this case to the fully nonlinear case O-4 in Table 5 that the M_2 constituent can be quite well-computed using only these iteratively updated linearized friction factors. The computed overtide responses, however, are dramatically different from the fully nonlinear case.

Table 5 indicates that the most significant forcings due to the finite amplitude term in the continuity equation occur at steady state and M_4. Basin-average continuity equation forcings at these harmonics are generated mainly due to the response at M_2 interacting with itself. The $\bar{P}_{\eta_j}$ forcings at M_2 and M_6 are much smaller than at steady state and M_4 since these forcings represent the interaction of the responses at M_2 with the much weaker overtide response at steady state and M_4. $\bar{P}_{\eta_j}$ at M_8 is even smaller than any of the previous harmonics since the interaction is now between even weaker overtides at higher frequencies with M_2 (e.g. M_6 with M_2) or between overtides with each other (e.g. M_4 with M_4). The finite amplitude continuity equation forcing at higher order harmonics progressively diminishes by about an order of magnitude with each higher frequency.

The responses at M_2 are not significantly affected by the finite amplitude forcing term due to the dominance of the boundary forcing and linear terms. Responses at each overtide are strictly determined by the amplitudes of the $\bar{P}_{\eta_j}$ forcing. Table 5 shows that the steady state response in average velocity is quite close to that

TABLE 5. Basin averaged harmonic forcings and responses for the M_2 astronomical boundary forcing case for various nonlinear interactions.

Case	Variable	Constituent					
		Steady	M_2	M_4	M_6	M_8	M_{10}
O-7	$\bar{P}_{\eta_j}$	28.368	4.9037	38.194	1.7947	0.13344	0.011926
	$\bar{P}_{U_j}$	0	0	0	0	0	0
	$\bar{\eta}_j$	0.00947	0.204	0.00387	0.000168	0.0000171	0.0000023
	$\bar{U}_j$	0.00356	0.128	0.00449	0.000319	0.0000305	0.0000037
O-8	$\bar{P}_{\eta_j}$	0	0	0	0	0	0
	$\bar{P}_{U_j}$	10^{-8}	2736.5	10^{-7}	269.96	10^{-7}	120.46
	$\bar{\eta}_j$	10^{-12}	0.208	10^{-12}	0.0109	10^{-12}	0.00473
	$\bar{U}_j$	10^{-12}	0.134	10^{-12}	0.0163	10^{-12}	0.00598
O-9	$\bar{P}_{\eta_j}$	0	0	0	0	0	0
	$\bar{P}_{U_j}$	51.595	2735.5	54.778	269.05	14.121	119.89
	$\bar{\eta}_j$	0.00677	0.208	0.00253	0.0109	0.000450	0.00472
	$\bar{U}_j$	0.000808	0.134	0.00367	0.0162	0.000791	0.00594
O-10	$\bar{P}_{\eta_j}$	28.988	5.1201	37.815	1.9809	3.8698	0.49813
	$\bar{P}_{U_j}$	100.02	2733.1	123.67	264.35	36.099	117.45
	$\bar{\eta}_j$	0.0126	0.208	0.00559	0.0108	0.00133	0.00465
	$\bar{U}_j$	0.00392	0.134	0.00541	0.0161	0.00181	0.00585
O-11	$\bar{P}_{\eta_j}$	28.890	5.8966	37.647	2.5238	3.8062	0.66956
	$\bar{P}_{U_j}$	150.37	2731.1	175.46	259.36	48.726	114.28
	$\bar{\eta}_j$	0.0193	0.208	0.00804	0.0106	0.00174	0.00455
	$\bar{U}_j$	0.00374	0.134	0.00770	0.0158	0.00250	0.00567
O-4	$\bar{P}_{\eta_j}$	28.872	5.8927	37.592	2.5364	3.7978	0.69860
	$\bar{P}_{U_j}$	155.44	2729.5	163.22	259.82	52.114	113.43
	$\bar{\eta}_j$	0.0204	0.208	0.00802	0.0106	0.00189	0.00454
	$\bar{U}_j$	0.00407	0.134	0.00811	0.0158	0.00274	0.00564

of the fully nonlinear run O-4 whereas the response in average elevation is about half. At M_4 both average responses in elevation and velocity appear to be about half as large as the fully nonlinear case. At M_6 responses are more than two orders of magnitude smaller than for the fully nonlinear case and for higher order harmonics this difference becomes progressively larger.

2) CASE O-8: QUADRATIC FRICTION WITH NO FINITE AMPLITUDE OR CONVECTIVE ACCELERATION EFFECTS

In this case we shall consider quadratic friction as the only nonlinear term and suppress all finite amplitude effects in both the continuity and momentum equations in addition to convective acceleration effects. Thus as Table 5 indicates, all harmonic nonlinear continuity equation forcings, $\bar{P}_{\eta_j}$, are equal to zero. Furthermore, as expected, harmonic nonlinear momentum equation forcings, $\bar{P}_{U_j}$, essentially occur only at odd harmonics M_2, M_6 and M_{10}. The forcings and responses at the odd overtide harmonics M_6 and M_{10} do not diminish as rapidly as those associated with the finite amplitude term in the previous case. This is due to the form of the friction term, $u|u|$, which is largely responsible for forcing all these odd harmonics simultaneously through the interaction of the M_2 response with itself. The largest harmonic nonlinear momentum equation forcing component is at the forcing frequency itself. This explains our success in approximating the friction term in the previous case by using information from a Fourier expansion of the dominant component of this term and a few simple linear iterations. The next largest value of $\bar{P}_{U_j}$ is found at M_6 and is an order of magnitude smaller than at M_2: $\bar{P}_{U_j}$ then progressively decreases by a factor of roughly two at each higher order odd harmonic. The extremely small momentum equation forcings at the even harmonics (steady state, M_4 and M_8) fall within the error threshold of the LSQ analysis procedure.

Table 5 shows that the M_2 basin averaged responses are almost identical to the fully nonlinear case O-4. The odd overtide harmonics, M_6 and M_{10}, have responses which are slightly higher than the fully nonlinear case. The responses at all even harmonics are essentially zero.

3) CASE O-9: QUADRATIC FRICTION INCLUDING FINITE AMPLITUDE IN THE MOMENTUM EQUATION ONLY

This case takes into account the full nonlinear friction term with finite amplitude but neglects finite amplitude effects in the continuity equation and convective acceleration terms. Table 5 indicates that nonlinear momentum equation forcings at the odd harmonics have remained essentially the same as in the previous case. However, now the finite amplitude component of the friction term generates nonlinear momentum equation forcings at the even harmonics which are, in general, much smaller than the forcings at the adjacent odd harmonics. These even harmonic forcings progressively decrease by about a factor of four, a much slower rate than in case O-7 with finite amplitude in the continuity equation acting alone. This is due to the fact that all these even harmonics are for a large part generated by the M_2 tide interacting with itself, as was the case for the odd harmonics generated with friction.

The responses at M_2 are essentially identical to both the previous case and the fully nonlinear case O-4. Odd harmonic responses are also the same as in the previous case, still slightly higher than in the fully nonlinear case. Even harmonic responses are all substantially smaller (between a factor of three to four) than the fully nonlinear case. When comparing even harmonic responses to the continuity equation finite amplitude only case O-7, we find that the comparisons vary quite a bit. The steady state response is much smaller, by a factor of five, compared to that of case O-7, whereas the M_4 response is comparable (to within a factor of 1.5) and the M_8 response is larger by a factor of 27. The substantial increase at M_8 is a result of the fully nonlinear friction term with finite amplitude directly generating a forcing at this constituent through M_2 interacting with itself.

4) CASE O-10: QUADRATIC FRICTION EXCLUDING FINITE AMPLITUDE IN THE MOMENTUM EQUATION BUT INCLUDING FINITE AMPLITUDE IN THE CONTINUITY EQUATION

We now consider quadratic friction in addition to finite amplitude in the continuity equation but do not compute finite amplitude terms in the momentum equation and convective acceleration terms. Again Table 5 shows that the nonlinear momentum equation forcings, $\bar{P}_{U_j}$, at the odd harmonics are almost the same as the previous two cases, showing slight decreases. The $\bar{P}_{U_j}$ values have doubled at the even harmonics compared to the previous case even though the finite amplitude part of the friction term has been turned off. These even harmonic $\bar{P}_{U_j}$ forcings are generated due to the responses existing at these frequencies themselves. These responses in turn were generated by the continuity equation finite amplitude forcings: $\bar{P}_{\eta_j}$ values for the steady state through M_6 harmonics are approximately the same as the continuity equation finite amplitude only case O-7. However, at M_8 and M_{10} we see an increase in $\bar{P}_{\eta_j}$ of more than an order of magnitude over case O-7.

Again the M_2 response is the same as the previous case and the fully nonlinear case O-4. Furthermore, odd harmonic responses have been slightly reduced from the previous nonlinear friction only cases although these responses are still slightly larger than the fully nonlinear case. Finally, although even harmonic responses are still somewhat under those of the fully nonlinear case, they are the correct order of magnitude and are in fact closer to the fully nonlinear run O-4 responses than any of the previous cases considered in this subsection. In particular, the M_8 response has increased by two orders of magnitude over the finite amplitude only case and by a factor of about three over the quadratic friction with finite amplitude in momentum only case O-9. This increased response at M_8 is no longer due to the largely simultaneous forcing of the even harmonics through M_2 interacting with itself, due to the form of the nonlinearity as in the previous case O-9, but results from the interaction through the continuity finite amplitude term of the M_2 and M_6 constituents as in case O-7. However, in the present case the M_6 response has been dramatically increased over that of case O-7 by two orders of magnitude due to the nonlinear friction term. Thus the large M_8 response is a result of the quadratic friction term generating a significant response at M_6 and the continuity finite amplitude term allowing the interaction of the M_2 and M_6 constituents to generate this response at M_8.

5) CASE O-11: QUADRATIC FRICTION WITH FINITE AMPLITUDE IN THE MOMENTUM AND CONTINUITY EQUATIONS

In this case we neglect only the convective acceleration terms: $\bar{P}_{U_j}$ forcings at odd harmonics continue to decrease slightly over the previous three cases. At even harmonics, $\bar{P}_{U_j}$ forcings have essentially increased over the previous two separate finite amplitude and quadratic friction cases as the sum of the average forcing values of these runs. Furthermore, $\bar{P}_{\eta_j}$ values are roughly the same at all even harmonics and are increased somewhat at odd harmonics compared to the previous case.

As Table 5 shows, responses at M_2 are again the same. Responses at odd overtide harmonics have continued to decrease slightly over the previous two cases and are now essentially equal to the fully nonlinear case O-4. This is a result of the fact that at these odd overtide harmonics the finite amplitude continuity equation forcing and the quadratic friction forcing are for a large part out of phase within the bight and thus add destructively. Average responses at even harmonics

add almost linearly from the responses at the previous two cases which considered the two finite amplitude terms separately in conjunction with friction. Thus, the finite amplitude effects in the continuity and momentum equations reinforce each other constructively at the even harmonics. For the generation of the steady state and M_4 tides, the finite amplitude term in the continuity equation is somewhat more important than the finite amplitude component of the nonlinear friction term. The M_8 tide is generated as a result of the mutual interaction of quadratic friction and continuity finite amplitude in addition to the finite amplitude portion of the friction term.

6) CASE O-4: ALL NONLINEAR TERMS COMPUTED

This fully nonlinear case considers quadratic friction, finite amplitude in both the momentum and continuity equations, and convective acceleration effects. Nonlinear forcings are about the same as the previous case with the exception of small changes in $\bar{P}_{U_j}$ at steady state, M_4 and M_8. Accordingly, small increases in even harmonic responses are seen due to the inclusion of convective acceleration.

c. *Overtide interactions*

Let us now examine to what extent the higher order overtides interact and influence the lower order overtides. We accomplish this by suppressing the feedback of the M_8 and/or M_{10} overtides into the response signal. In this series of three cases we initially allow the interaction of the steady state through M_6 constituents and then add the M_8 and M_{10} harmonics to interact with the other harmonics. All nonlinearities are computed and a c_f value of 0.0095 is used. The harmonic basin averaged responses for these cases are given in Table 6.

It is noted that the responses at steady state, M_4 and M_6 are all increased by the inclusion of the combined M_8 and M_{10} constituents. The changes in response typically alternate somewhat depending on whether we have added an even or odd harmonic. As much as a 6% increase is seen in the M_6 response due to the interaction with the M_{10} tide. Furthermore, case O-13 shows that the M_{10} constituent also interacts with M_8 through the continuity finite amplitude term and decreases the response at M_8 by about 11%. Responses at M_4 and M_6 will not change significantly with the addition of constituents higher than M_{10}. However, slight changes will still occur at M_8 and M_{10} due to the addition of the M_{12} and M_{14} constituents.

d. *Summary of the nonlinear overtide interactions*

We have examined some aspects of the overtide interactions within the Bight of Abaco. The dominant nonlinearity is quadratic friction and the sill region is the most important area with respect to the generation and interaction of the main M_2 tide and its overtides. Thus the optimal global friction factor of $c_f = 0.0095$, which is physically well justified in the sill area, leads to very satisfactory comparison to measurement data for the M_2 and M_4 constituents. The M_6 tide, however, is substantially overpredicted.

We have determined the influence of the various nonlinear terms in controlling the response at each frequency. The M_2 tide is entirely dominated by quadratic friction. However, this quadratic friction is largely linear with regard to its behavior at M_2 itself. Therefore M_2 can be well modeled with a linear friction law as long as local λ values are properly determined. The M_2 constituent is not significantly affected by finite amplitude in either the continuity or momentum equations or by convective acceleration. However, the M_2 responses are one of the most critical factors in determining the generation of the overtides. The steady state response is mainly caused by the finite amplitude term in the continuity equation in addition to a smaller constructive contribution from the finite amplitude portion of the nonlinear friction term and a small constructive contribution from convective acceleration. The M_4 constituent is primarily generated by the continuity finite amplitude forcing together with a secondary but similar order constructive forcing due to the finite amplitude component of the friction term. This constructive addition is due to the highly coherent phase between these two forcings at M_4. The M_6 con-

TABLE 6. Basin averaged harmonic responses for the M_2 astronomical boundary forcing case and varying degree of overtide interaction.

		Constituent					
Case	Variable	Steady	M_2	M_4	M_6	M_8	M_{10}
O-12	$\bar{\eta}_j$	0.0208	0.208	0.00792	0.00999	—	—
	$\bar{U}_j$	0.00404	0.134	0.00793	0.0151	—	—
O-13	$\bar{\eta}_j$	0.0198	0.208	0.00812	0.00998	0.00206	—
	$\bar{U}_j$	0.00410	0.134	0.00831	0.0151	0.00308	—
O-4	$\bar{\eta}_j$	0.0204	0.208	0.00802	0.0106	0.00189	0.00454
	$\bar{U}_j$	0.00407	0.134	0.00811	0.0158	0.00274	0.00564

stituent is almost entirely generated by the quadratic friction term with a small destructive contribution from the finite amplitude term in the continuity equation due to these two forcings being out of phase over a large area of the basin. The M_8 tide is generated largely through the continuity finite amplitude term but is dependent on the relatively high response existing at M_6 which can only be generated through the quadratic friction law. The M_8 tide is further influenced directly by the finite amplitude portion of the friction term in addition to a small effect of the convective acceleration terms. Finally, the M_{10} constituent is generated mainly by the quadratic friction term but sees a small reduction in response due to the out of phase forcing of the finite amplitude term.

Though M_2 is largely responsible for directly forcing many of the nonlinear tides, there are also interactions between the main M_2 tide and its overtides which can significantly influence the responses at other overtides. The generation of the M_8 constituent is, of course, the most dramatic example of this. However, we also saw that the influence of higher order harmonics such as the M_8 and M_{10} can respectively increase responses at the M_4 and M_6 constituents.

Finally, by showing that the convective acceleration terms were not very important we can justify our neglecting the eddy viscosity type terms in our computations since it is reasonable to assume that lateral turbulent momentum transport is closely related to the convective terms. Of course this does assume that the depth averaging used in our formulation does not significantly contribute to these dispersion type terms.

5. Compound-tide computations

Let us now examine the nonlinear interactions and generated shallow water tides which appear through the simultaneous boundary forcing of all five measured astronomical constituents. Some of the details of these interactions will be determined through a series of runs which selectively bring into the full nonlinear interaction groups of astronomical and/or compound tide constituents. The first compound tide case C-1 in this section takes into consideration M_2 and its overtides in addition to the K_1, O_1, N_2 and S_2 astronomical constituents. All compound tide constituents are suppressed by not computing responses at these constituents and thus not allowing the suppressed constituents to feed into the time history responses and nonlinear forcing vectors. Subsequent cases, in addition, allow the interaction of sets of compound tides grouped according to the astronomical constituents which generated them. In case C-2, M_2–N_2 compound tides are allowed to interact with all astronomical tides, the M_2 overtides and with themselves, while the interaction with all other compound tides is still constrained. The remaining runs progressively take into account the M_2–S_2 compound tides, the M_2–N_2–S_2 compound tides and finally compound tides involving the O_1 and K_1 tides.

The harmonics considered in our compound tide computations are listed in Table 7. These tidal constituents result from the nonlinear interaction between the five astronomical constituents considered and may be significant within the Bight of Abaco. Although the K_2 constituent is normally considered to be an astronomical constituent, it is treated here as a pure overtide of the K_1 astronomical tide. Furthermore the SO_3 and MK_3 constituents have identical associated frequencies and are therefore not separable in our computations.

The LSQ harmonic analysis is always performed using all the frequencies listed in Table 7 regardless of

TABLE 7. List of frequencies used for compound tide cases (cases C-1 through C-5)

Tide	Frequency (rad s^{-1})	Period (h)
Steady	0.000000000000000	—
MN	0.000002639203296	661.31
SM	0.000004925202335	354.37
O_1	0.000067597751162	25.82
K_1	0.000072921165921	23.93
SO_1	0.000077846368256	22.42
MNS_2	0.000132954511452	13.13
$2MK_2$	0.000135195502324	12.91
$2NM_2$	0.000135240510491	12.91
$2MS_2$	0.000135593714748	12.87
N_2	0.000137879713787	12.66
$3MSN_2$	0.000138232918044	12.63
M_2	0.000140518917083	12.42
SNM_2	0.000142804916122	12.22
$2MN_2$	0.000143158120379	12.19
S_2	0.000145444119418	12.00
K_2	0.000145842331842	11.97
MSN_2	0.000148083322714	11.79
$2SM_2$	0.000150369321753	11.61
MO_3	0.000208116668245	8.39
SO_3 and MK_3	0.000213041870580	8.19
KO_3	0.000213440083004	8.18
SK_3	0.000218365285339	7.99
$2MNS_4$	0.000273473428535	6.38
N_4	0.000275759427574	6.33
$3MS_4$	0.000276112631831	6.32
MN_4	0.000278398630870	6.27
M_4	0.000281037834166	6.21
$3MN_4$	0.000283677037462	6.15
MS_4	0.000285963036501	6.10
MK_4	0.000286361248925	6.09
$2MSN_4$	0.000288602239797	6.05
$2NM_6$	0.000416278344658	4.19
$2MN_6$	0.000418917547953	4.17
M_6	0.000421556751249	4.14
MSN_6	0.000423842750288	4.12
$2MS_6$	0.000426481953584	4.09
$2MK_6$	0.000426880166008	4.09
$2SM_6$	0.000431407155919	4.05
$2(MN)_8$	0.000556797261741	3.13
$3MN_8$	0.000559436465036	3.12
M_8	0.000562075668332	3.11
$2MSN_8$	0.000564361667371	3.09
$3MS_8$	0.000567000870667	3.08
M_{10}	0.000702594585415	2.48

the constituents which are suppressed in any given case. This is done to ensure the accuracy of the LSQ analysis, since despite the fact that certain nonlinear interactions may be suppressed, there will be nonlinear forcings at all these frequencies because all five astronomical constituents are always allowed to interact through the nonlinearities. A central time origin and 394 evenly spaced time sampling points, 8.39078505 days apart, were used for the LSQ harmonic analysis. This leads to a time sampling record length of 9.03 years which is about twice as long as the maximum synodic period of 4.43 years for this set of frequencies. It is noted that a standard hourly LSQ analysis would involve 100 to 200 times more time points than our tailored LSQ analysis for the same resolution capability.

Open ocean boundary forcings for the five astronomical constituents are uniformly applied across this boundary using the values in Table 1. Elevations for all the interacting nonlinear constituents on this boundary are set to zero. Furthermore, all cases in this section include all nonlinearities and use a friction value of $c_f = 0.0095$.

Basin averaged elevation responses, $\bar{\eta}_j$, for the five cases considered in this section in addition to responses for case O-4 are presented in Table 8. However, only constituents with $\bar{\eta}_j$ values above a threshold of 0.001 m are considered to be significant and reported. In general, it is not even necessary to compute these below threshold constituents since their effect on most significant constituents is usually very small.

We now proceed to discuss the cases at hand. We shall note significant changes in the computed tides as we progressively take more constituents into account with each case. In addition to conclusions drawn from these five cases we will present major conclusions or observations from cases which selectively suppress certain astronomical tides, compound tides or nonlinearities but which are not presented in detail.

a. Case C-1: Nonlinear interaction of the O_1, K_1, M_2, N_2 and S_2 astronomical tides and M_2 overtides

In addition to M_2 and its overtides (case O-4), we now consider the interaction of the four secondary astronomical tides. Certainly these secondary astronomical constituents are much less important than the primary M_2 tide. Computed basin average elevation responses in Table 8 indicate that the values for $\bar{\eta}_j$ at K_1, O_1 and N_2 are respectively 28%, 24% and 20% of $\bar{\eta}_j$ at M_2, while the average S_2 response is only 12% of the average M_2 response.

The introduction of the four secondary astronomical tides only slightly influences the primary M_2 tide. By comparing the responses of case C-1 to case O-4 in Table 8 it is noted that $\bar{\eta}_j$ at M_2 only decreases by 2%. The M_2 overtides are however substantially influenced. Table 8 indicates that compared to case O-4, $\bar{\eta}_j$ at M_4 has decreased by 5% and $\bar{\eta}_j$ values at M_6, M_8 and M_{10} have decreased respectively by 13%, 17% and 23%. From computations not presented, which add only the N_2 and/or S_2 constituents to the harmonics of case O-4, it was deduced that the largest portion of these

TABLE 8. Basin-average harmonic elevation responses (in meters) for compound tide cases. Only harmonics with significant responses are included. Suppressed constituents are indicated by "—".

Case	O-4	C-1	C-2	C-3	C-4	C-5
Steady	0.0204	0.0195	0.0195	0.0194	0.0194	0.0203
MN	—	—	0.0116	0.0115	0.0114	0.0114
SM	—	—	—	0.00684	0.00680	0.00717
O_1	—	0.0482	0.0479	0.0479	0.0479	0.0483
K_1	—	0.0567	0.0565	0.0564	0.0564	0.0576
MNS_2	—	—	—	—	0.00109	0.00107
$2MS_2$	—	—	—	0.00401	0.00413	0.00407
N_2	—	0.0414	0.0442	0.0441	0.0443	0.0442
$3MSN_2$	—	—	—	—	0.00103	0.00101
M_2	0.208	0.204	0.204	0.204	0.204	0.204
SNM_2	—	—	—	—	0.00102	0.00114
$2MN_2$	—	—	0.00676	0.00668	0.00673	0.00665
S_2	—	0.0243	0.0243	0.0258	0.0261	0.0261
K_2	—	—	—	—	—	0.00111
MO_3	—	—	—	—	—	0.00224
KO_3	—	—	—	—	—	0.00189
MN_4	—	—	0.00353	0.00352	0.00353	0.00353
M_4	0.00802	0.00760	0.00748	0.00742	0.00741	0.00746
MS_4	—	—	—	0.00213	0.00213	0.00217
$2MN_6$	—	—	0.00401	0.00396	0.00398	0.00395
M_6	0.0106	0.00920	0.00840	0.00816	0.00812	0.00785
$2MS_6$	—	—	—	0.00232	0.00237	0.00233
$3MN_8$	—	—	0.00119	0.00119	0.00118	0.00118
M_8	0.00189	0.00157	0.00139	0.00133	0.00133	0.00132
M_{10}	0.00454	0.00348	0.00281	0.00262	0.00261	0.00244

changes is due to the diurnal constituents. This is related to the mixed character of the tides in the bight. For the main M_2 tide and the odd overtide harmonics, M_6 and M_{10}, more than half the decreases in amplitude can be attributed to the O_1 and K_1 tides, whereas for the even harmonics, M_4 and M_8, the relative changes in amplitude are almost entirely due to the diurnal tides. The response decreases attributed to the semidiurnal secondary astronomical tides are dominated by the N_2 constituent. Furthermore, these additional computations indicate that the semidiurnal N_2 and S_2 constituents were themselves not substantially influenced by the diurnal tides (changes less than 1%) indicating a limited direct interaction between these secondary astronomical constituents themselves.

Quadratic friction is the primary mechanism through which the various secondary astronomical constituents interact with the dominant M_2 tide. In fact, additional computations indicate that all the secondary constituents are substantially reduced (between 14% and 20%) through the nonlinear quadratic friction terms when compared to linearized friction computations. These frictional decreases are somewhat offset by small increases due to the finite amplitude terms for the O_1 and K_1 constituents. The decreases in M_2 and its odd overtides noted between cases O-4 and C-1 are directly related to the significant changes in the frictional balance in the bight, which occur when the secondary astronomical tides are taken into account. The small decrease seen in the M_4 tide can be attributed to the small decrease in the M_2 response, which is almost entirely responsible for driving the M_4 through the finite amplitude terms. The much more significant decrease in the M_8 tide is related to the small drop in M_2 and the much greater decrease in M_6 which combine to generate the M_8 constituent.

b. *Case C-2: Addition of the M_2–N_2 compound tides*

We now include the full nonlinear interaction of the M_2–N_2 compound tides to the interacting constituents considered in case C-1. Significant M_2–N_2 compound tides which appear are the MN, $2MN_2$, MN_4, $2MN_6$ and $3MN_8$ tides. The MN and MN_4 are generated through the finite amplitude terms, the $2MN_2$ is generated almost entirely through the quadratic friction term and the $2MN_6$ is dominantly generated by quadratic friction with a small destructive contribution from the continuity equation finite amplitude term. The $3MN_8$ constituent, in a manner analogous to M_8, is generated through the combined influence of quadratic friction generating a high response at M_6 and the continuity finite amplitude term allowing a direct interaction between N_2 and M_6. Table 8 indicates that the M_2–N_2 compound tides typically have a basin-average elevation amplitude of a little less than half the corresponding M_2 overtide with the exception of $3MN_8$ which has an average amplitude of 86% of the adjacent M_8. The most important M_2–N_2 compound tide, the $2MN_2$ constituent, has no associated adjacent M_2 overtide.

As is seen from Table 8, the majority of the astronomical constituents remain essentially unchanged when the nonlinear interactions involving the M_2–N_2 compound tides are considered. A notable exception is the N_2 astronomical constituent which increases by 7% compared to case C-1. The M_2 overtides again experience substantial drops in $\bar{\eta}_j$. While the M_4 only decreases by less than 2% due to the inclusion of the M_2–N_2 compound tides, the M_6, M_8 and M_{10} tides see decreases in $\bar{\eta}_j$ of respectively 9%, 11% and 19%. It can be demonstrated that it is the $2MN_2$ tide which is chiefly responsible for these changes in the N_2 and M_2-overtide constituents. The $2MN_2$ constituent also significantly influences other M_2–N_2 compound tides (by up to 20%). All these factors indicate a relatively strong frictional interaction between $2MN_2$, M_2 and N_2 and the M_2 overtides.

From computations not presented here, which in the same way as case C-2 took into account M_2 and its overtides, S_2 and/or N_2, but suppressed the O_1 and K_1 constituents, it can be shown that the same relative changes that were noted between runs C-1 and C-2 occur once the M_2–N_2 compound tides were taken into account. However, these computations did indicate that some of the M_2–N_2 compound tides are influenced by the O_1 and K_1 tides (in particular the $2MN_6$ and $3MN_8$ responses were lowered by about 5%) while not being significantly influenced by the S_2 constituent. This influence of the O_1 and K_1 tides on the M_2–N_2 compound tides is related to the lowering of the M_2 overtides which results due to the presence of the O_1 and K_1 constituents.

c. *Case C-3: Addition of the M_2–S_2 compound tides*

In addition to the constituents considered in case C-2 we now take into account the full interaction of the M_2–S_2 compound tides. The significant M_2–S_2 compound tides which appear are the SM, $2MS_2$, MS_4 and $2MS_6$. The nonlinear mechanisms which generate these constituents are the same as for the corresponding M_2–N_2 compound tides.

Table 8 shows that the significant M_2–S_2 compound tides appear with only a little more than one-fourth of the basin-average elevation amplitude of the adjacent M_2 overtides. Thus the M_2–S_2 compound tides are about 40% smaller than the corresponding M_2–N_2 compound tides which is directly related to the smaller S_2 astronomical tide relative to the N_2 astronomical tide. The $2MS_2$ is the largest M_2–S_2 compound tide.

Taking the M_2–S_2 compound tide into account essentially does not affect any of the astronomical constituents with the exception of the S_2 tide. When comparing $\hat{\eta}_j$ at S_2 for this case to that of case C-2 in Table 8, we note an increase in S_2 of about 6% due to the

M_2–S_2 compound tides. This percentage increase is similar to that which N_2 saw when the M_2–N_2 compound tides were added. The inclusion of the M_2–S_2 tides further decreases the M_2 overtides: $\bar{\eta}_j$ at M_4 drops by less than 1% while M_6, M_8 and M_{10} decrease respectively by 3%, 4% and 7%. These decreases are quite a bit smaller than those experienced when the M_2–N_2 compound tides were added (in fact a third as small). This is again related to the smaller S_2 and associated M_2–S_2 compound tides in relation to the N_2 tide and its compound tides. The increase seen in the S_2 constituent and the decrease in the M_2 overtides are dominantly caused by compound tide frictional interactions involving the $2MS_2$ tide. In general, the characteristics of the M_2–S_2 compound tide interactions are very similar to those experienced with the M_2–N_2 interactions, except substantially smaller.

Finally, it is noted from Table 8 that the M_2–N_2 compound tides are only marginally affected by the M_2–S_2 compound tides. Through computations similar to case C-3 (except with N_2 and/or O_1 and K_1 interactions suppressed), it can be shown that the pattern of relative change brought about through the introduction of the M_2–S_2 compound constituents is identical to that of case C-3. However, in case C-3 the M_2–S_2 constituents were weakened by the O_1, K_1 and N_2 astronomical constituents in addition to the M_2–N_2 compound constituents. Whereas the M_2–N_2 compound tides were not significantly influenced by the M_2–S_2 compound tides, the reverse is not true. Again this is due to the much more substantial effect the M_2–N_2 compound tides have on the M_2 overtides.

d. Case C-4: Addition of the M_2–N_2–S_2 compound tides

We now include the interaction of compound tides which involve the M_2, N_2 and S_2 constituents. Three significant constituents of this type were computed: the SNM_2, $3MSN_2$ and MNS_2 tides. These semidiurnal compound tides are generated almost entirely by quadratic friction. These tides were the smallest significant constituents computed in this run and are only slightly above the 0.001 m threshold.

Comparing responses presented in Table 8 for this case to those of the previous case C-3 indicates that the M_2, O_1 and K_1 astronomical tides are not at all affected by these M_2–N_2–S_2 compound tides, while a very slight increase is seen in the N_2 and S_2 tides (respectively 0.5% and 1% increase). With the exception of a few M_2–S_2 compound tides no significant changes are noted in any of the nonlinear shallow water constituents. All of these interactions are quite weak due to the smallness of the M_2–N_2–S_2 compound tides.

From computations which were similar to case C-4, with the exception of suppressing O_1 and K_1, it was noted that certain M_2–N_2–S_2 compound tides are significantly affected by the O_1 and K_1 tides. In fact, the presence of the O_1 and K_1 constituents lowers these compound tides by as much as 23%. This substantial lowering is a result of the participation of not only the astronomical tides and M_2 overtides but also the M_2–N_2 and the M_2–S_2 compound tides in the generation of the M_2–N_2–S_2 compound tides. Thus since M_2 overtides and M_2–N_2 and M_2–S_2 compound tides all decrease due to the O_1 and K_1 tides, we see this dramatic decrease.

e. Case C-5: Addition of overtides and compound tides involving O_1 and K_1

Finally we shall consider the interaction of overtide and compound constituents involving the O_1 and K_1 tides with other constituents in addition to all the tides considered in the previous cases. Two relatively important terdiurnal tides now appear through the nonlinear interactions, the MO_3 and KO_3 tides. These constituents are generated by quadratic friction, although the responses are reduced significantly by both finite amplitude terms and to a much smaller degree by the convective acceleration terms. These terdiurnal constituents are both slightly smaller than the M_{10} tide. It is noted that the KO_3 tide is relatively important while not involving the primary M_2 tide. This is possible due to the O_1 and K_1 tides being the predominant secondary astronomical constituents. Finally, we note that a small K_2 overtide also appears which is slightly above the threshold of significance. The K_2 overtide is dominantly generated by quadratic friction although its response is somewhat reduced by both finite amplitude terms.

Checking Table 8 we see that M_2, N_2 and S_2 astronomical constituents do not change as a result of interactions with O_1/K_1 compound tides. The O_1 and K_1 astronomical tides do however increase by about 1% and 2%, respectively. The increases in these astronomical constituents are small compared to those experienced by the N_2 and S_2 constituents when their corresponding compound tides were added. Even though the $2MK_2$ tide has been included it certainly does not have the pronounced influence of the $2MN_2$ and $2MS_2$ tides. However, the $2MK_2$ constituent is very weak since it results from the interaction of the M_2 tide with the weak K_2 tide which is included in the computations only as an overtide of the K_1 constituent. The only M_2 overtides which are significantly influenced are the M_6 and M_{10}, which decrease by respectively 3% and 7% compared to case C-4. The M_2–N_2 compound tides see some very small changes while the M_2–S_2 compound tides are slightly more affected. The M_2–N_2–S_2 compound tides are also only slightly affected with the exception of SNM_2. In general, however, the interaction of O_1/K_1 compound tides with other compound tides is weak.

f. Summary of major features of compound tide runs

In this section we have seen that important nonlinear interactions and couplings occur between the astro-

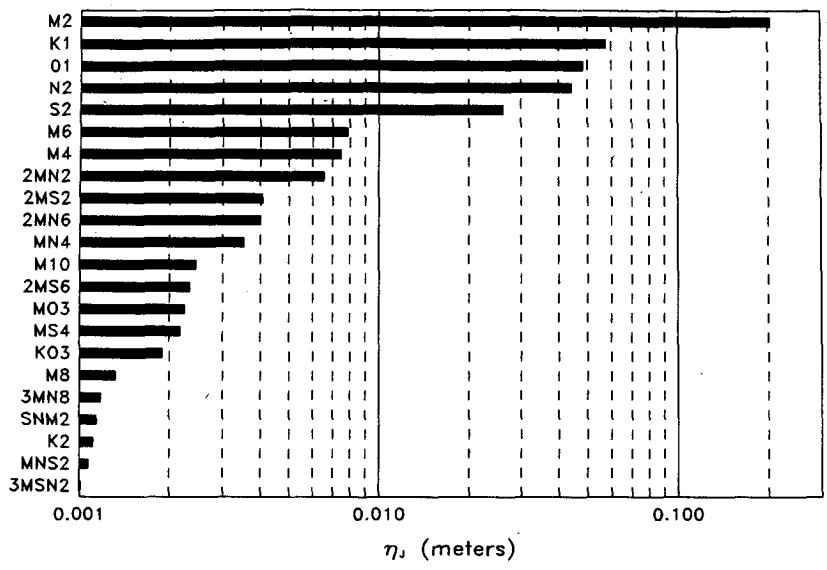

FIG. 4. Basin averaged elevation amplitudes (in meters) for significant constituents.

nomical and shallow water tides. The M_2 overtides have been especially significantly affected in our more detailed computations. Between case O-5 which considered only M_2 and its overtides and case C-5 which considers five astronomical constituents and all pertinent nonlinear tides, the M_4, M_6, M_8 and M_{10} respectively decrease by 7%, 26%, 30% and 46%. The addition of the secondary astronomical constituents are responsible for most of the decrease in M_4 and about half the change in M_6, M_8 and M_{10}. The inclusion of compound tides affects the M_4 very little but, as a whole, is responsible for the other half of the decrease in the M_6 through M_{10} overtides. Of all the compound tides, the $2MN_2$ is the most important. In fact this constituent brings about the single greatest decreases in the M_6, M_8 and M_{10} tides of any of the tides considered, whether astronomical or nonlinear with the exception of M_2. These decreases are through frictional interactions either directly, as is largely the case with the M_6 and M_{10} tides, or in conjunction with finite amplitude interactions, as is the case for the M_8 (through its dependence on M_6). Furthermore the relatively larger change in M_{10} indicates an important interaction between M_6 and M_{10}. Thus M_6 is affected by M_{10} as was noted in section 4, but M_{10} is also significantly affected by M_6.

Compound tides also significantly influence secondary astronomical constituents and other compound tides. In fact the presence of the $2MN_2$ and $2MS_2$ tides respectively increase the N_2 and S_2 astronomical constituents by about 7%. Furthermore these two important compound tides strongly interact with compound tides involving the same two astronomical tides. The $2MS_2$ is very similar to the $2MN_2$ but, in general, interacts less strongly due to the S_2 tide being smaller than the N_2 tide. Furthermore the strength of the compound tides are not only determined by the astronomical tides and compound tides of the same species but are also sensitive to the strength of the M_2 overtides. Thus, in general, mechanisms which affect the M_2 overtides will in turn affect the compound tides. Otherwise interactions between compound tides of different species appear to be weak.

Figure 4 shows the relative importance of significant constituents based on computed basin averaged elevations. We note that compound tides are important relative to the overall sequence of nonlinear constituents. We also note that the sexto-diurnal constituents are of about the same importance as the corresponding

TABLE 9. Elevation amplitude measurement error for each constituent in terms of proportional standard deviation, S_j^m.

	Constituent						
	O_1	K_1	N_2	M_2	S_2	M_4	M_6
S_j^m	0.03	0.08	0.13	0.03	0.14	0.10	0.12

TABLE 10. Elevation amplitude prediction error, S_j^p, for runs which vary friction factor, c_f, for overtide computations.

		Constituent		
Case	c_f	M_2	M_4	M_6
O-1	0.0030	0.5044	1.1306	1.6045
O-2	0.0060	0.1954	0.4655	1.2342
O-3	0.0090	0.0923	0.2923	1.0194
O-4	0.0095	0.0893	0.2853	0.9929
O-5	0.0100	0.0899	0.2823	0.9683
O-6	0.0120	0.1122	0.2958	0.8867

TABLE 11. Elevation amplitude prediction error, S_j^p, for compound tide cases.

	Constituent						
Case	O_1	K_1	N_2	M_2	S_2	M_4	M_6
O-4	—	—	—	0.0893	—	0.2853	0.9929
C-1	0.1594	0.1623	0.1962	0.0899	0.2684	0.2805	0.7471
C-2	0.1635	0.1649	0.1847	0.0900	0.2698	0.2777	0.6051
C-3	0.1637	0.1659	0.1848	0.0900	0.2323	0.2771	0.5640
C-4	0.1641	0.1661	0.1848	0.0901	0.2257	0.2770	0.5579
C-5	0.1564	0.1486	0.1850	0.0901	0.2254	0.2768	0.5128

quarter-diurnal constituents (i.e. $\bar{\eta}_{M_6} \approx \bar{\eta}_{M_4}$; $\bar{\eta}_{2MN_6} \approx \bar{\eta}_{MN_4}$; etc.). This is related to the very shallow depths in the bight and the dominance of the associated frictional interactions.

In general, the amplitudes of all the nonlinear constituents are quite small. However, the astronomical constituents are relatively small as well and it can be shown that the ratios of the amplitudes of the various constituents to that of the M_2 constituent in the Bight of Abaco are of similar order as in more energetic basins such as the English Channel. Thus it is anticipated that the same dynamic interactions discussed in this paper also occur in other very shallow basins with a dominating M_2 tide.

Finally, we note that low frequency constituents (steady state, MN and SM) are not included in Fig. 4 since, as was indicated earlier, these constituents would incorrectly appear as too significant when ranked in terms of $\bar{\eta}_j$. Based on the importance of $\bar{U}_j$, the sequence of constituents listed would remain approximately the same while the low frequency constituents would appear as follows: steady state would be slightly smaller than $2MN_6$; MN would be smaller than KO_3; SM would be smaller than $3MSN_2$.

6. Comparison of TEA-NL computations to measurement data

Filloux and Snyder (1979) carried out extensive measurements of water surface elevation within the bight. In a sequence of three field experiments, each lasting approximately one month, bottom mounted pressure gauges collected elevation time history records at a total of 25 sites (shown in Fig. 2). The month long elevation records for each experiment were harmonically decomposed using the least squares method in addition to being adjusted for atmospheric pressure, to yield harmonic elevation amplitudes and phases for the M_2, N_2, S_2, O_1, K_1, M_4 and M_6 constituents. Since only 15 gauges were deployed during any one experiment, each site has associated with it between one to three values for the seven harmonic constituents. However, there is a degree of variability from experiment to experiment in these harmonically decomposed measured values. In order to quantify this variability, we computed the proportional standard deviation, on a basin wide basis, for the amplitudes of each of the seven constituents which resulted from Filloux and Snyder's measurements. This proportional standard deviation of measurement data for each harmonic constituent j is expressed as:

$$S_j^m = \left[\frac{\sum_{l=1}^{L'} \sum_{k=1}^{K_l} [\hat{\eta}_j^m(x_l, k) - \frac{1}{K_l} \sum_{k=1}^{K_l} \hat{\eta}_j^m(x_l, k)]^2}{\sum_{l=1}^{L'} \sum_{k=1}^{K_l} [\hat{\eta}_j^m(x_l, k)]^2} \right]^{1/2},$$

where,

- $\hat{\eta}_j^m$ measured elevation amplitude component for jth harmonic
- x_l measurement site within the bight
- L' total number of measurement sites with multiple values for a constituent
- K_l total number of harmonically analyzed measurement values at location l.

The S_j^m values presented in Table 9 may be interpreted as the standard deviation in terms of a fraction of a

TABLE 12. Elevation amplitude prediction error, S_j^p, for reoptimization of c_f with full compound tide interaction.

		Constituent						
Case	c_f	O_1	K_1	N_2	M_2	S_2	M_4	M_6
C-5	0.0095	0.1564	0.1486	0.1850	0.0901	0.2254	0.2768	0.5128
C-6	0.0090	0.1432	0.1371	0.1849	0.0890	0.2175	0.2740	0.5296
C-7	0.0085	0.1293	0.1256	0.1863	0.0918	0.2097	0.2752	0.5484
C-8	0.0080	0.1150	0.1147	0.1894	0.0990	0.2022	0.2818	0.5695

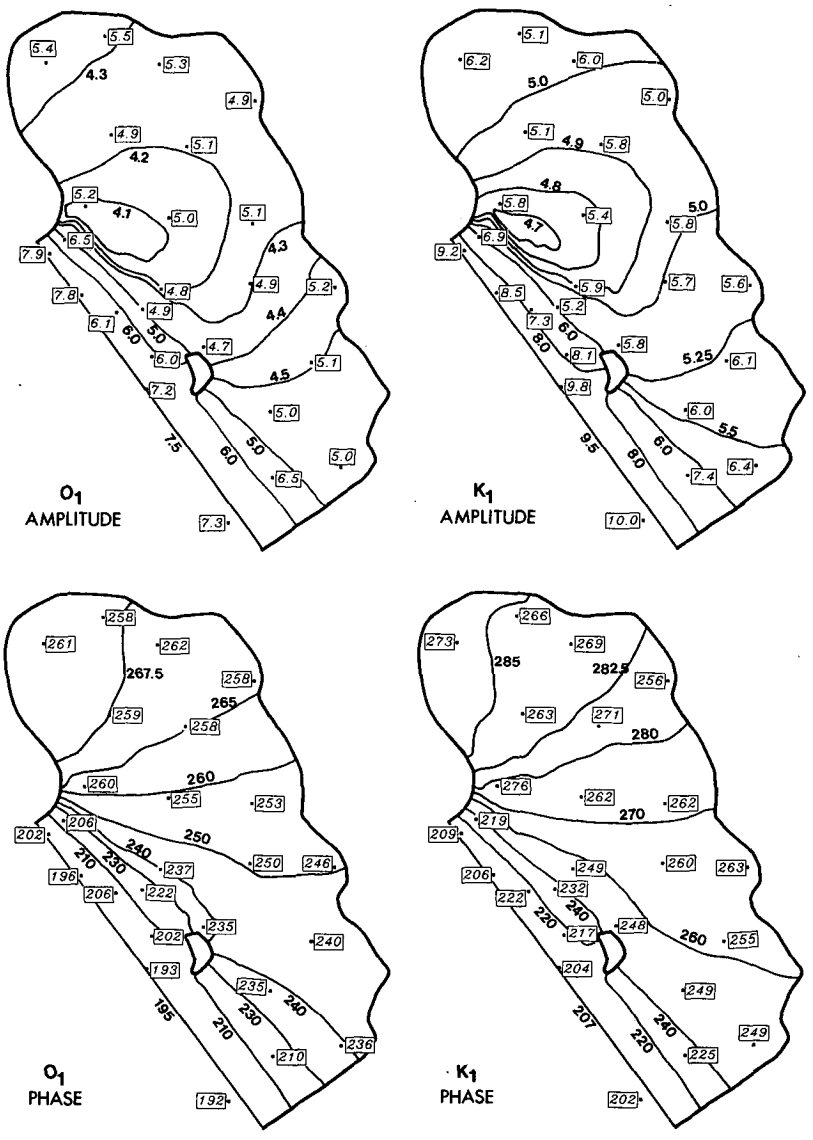

FIG. 5. Computed contours and average measured (boxed) values for elevation amplitudes (in cm) and phases (in degrees lag w.r.t. the M_2 constituent at the open ocean boundary) for the astronomical constituents for case C-6.

global representative measure of amplitude or roughly as an average percentage of error for each constituent.

In order to compare TEA-NL computations to these measured values, we shall compute the proportional standard deviation between predicted elevation amplitude and measurement elevation amplitude for each harmonic j in the same way as Snyder et al. (1979):

$$S_j^p = \left[\frac{\sum_{l=1}^{L} \sum_{k=1}^{K_l} [\hat{\eta}_j{}^m(x_l, k) - \hat{\eta}_j(x_l)]^2}{\sum_{l=1}^{L} \sum_{k=1}^{K_l} [\hat{\eta}_j{}^m(x_l, k)]^2} \right]^{1/2},$$

where $\hat{\eta}_j$ is the TEA-NL predicted elevation amplitude component for the jth harmonic, and L the total number of measurement sites. Again these values will represent the average standard deviation for a given constituent in terms of a fraction of the global representative measure of amplitude. It is noted that this prediction error, S_j^p, incorporates the measurement errors. Let us now look how the various computations discussed in sections 4 and 5 influence the prediction error, S_j^p.

a. Error dependence on friction factor, c_f, for the overtide computations

In section 4, we varied friction factor c_f to determine its influence on M_2 and its overtides. Table 10 now shows how well these friction factors allow the predic-

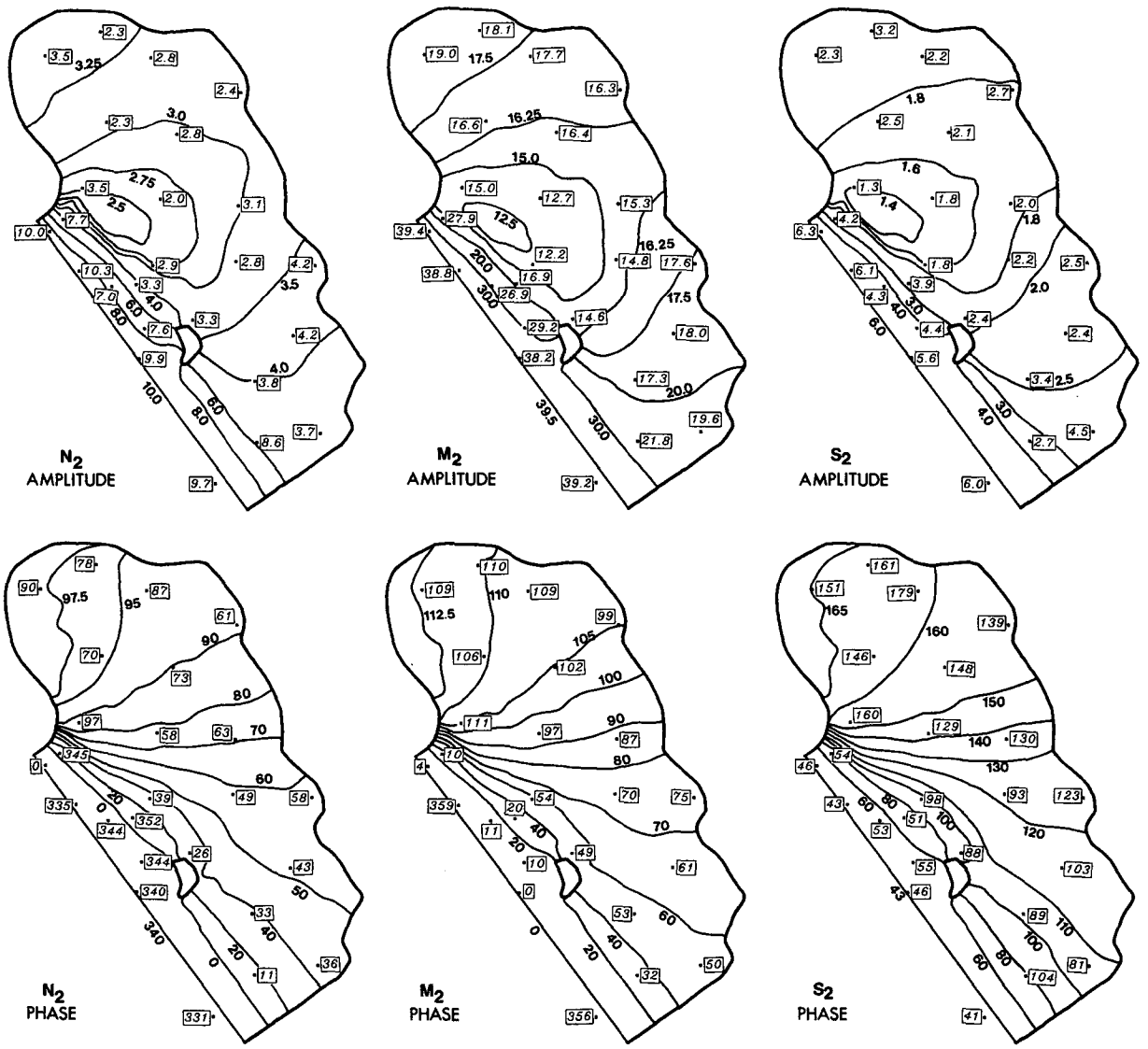

FIG 5. (*Continued*)

tion of the M_2, M_4 and M_6 constituents in these overtide only cases with all nonlinearities turned on. Clearly the optimum M_2 response occurs at $c_f = 0.0095$. At this friction factor value there is on average a 9% error between TEA-NL predictions and Filloux and Snyder's (1979) measurements. The M_4 error appears to be a near minimum at $c_f = 0.0095$ with an error of $S_j^p \approx 29\%$. A slightly higher c_f value yields a small reduction in the S_j^p value for this constituent. The M_6 errors continue to decrease over the entire range of c_f values tested. At $c_f = 0.0095$ the M_6 elevation amplitude is entirely overpredicted by approximately 99% or by roughly a factor of two. The final optimal friction factor selected in section 4 was based solely on the lowest elevation amplitude error for the main M_2 tide.

b. Error dependence on compound tide interactions with $c_f = 0.0095$

In section 5, we investigated the variation of responses due to the influence of the interactions between various astronomical and nonlinear compound tide constituents. Table 11 indicates the associated elevation amplitude prediction errors in terms of S_j^p. We shall now point out the key features of these cases which progressively allow more and more constituents to interact.

Comparing cases O-4 and C-1, we note that allowing the O_1, K_1, N_2 and S_2 astronomical constituents to interact substantially reduces the M_6 overprediction in elevation amplitude from 99.3% to 74.7%. The M_2 and

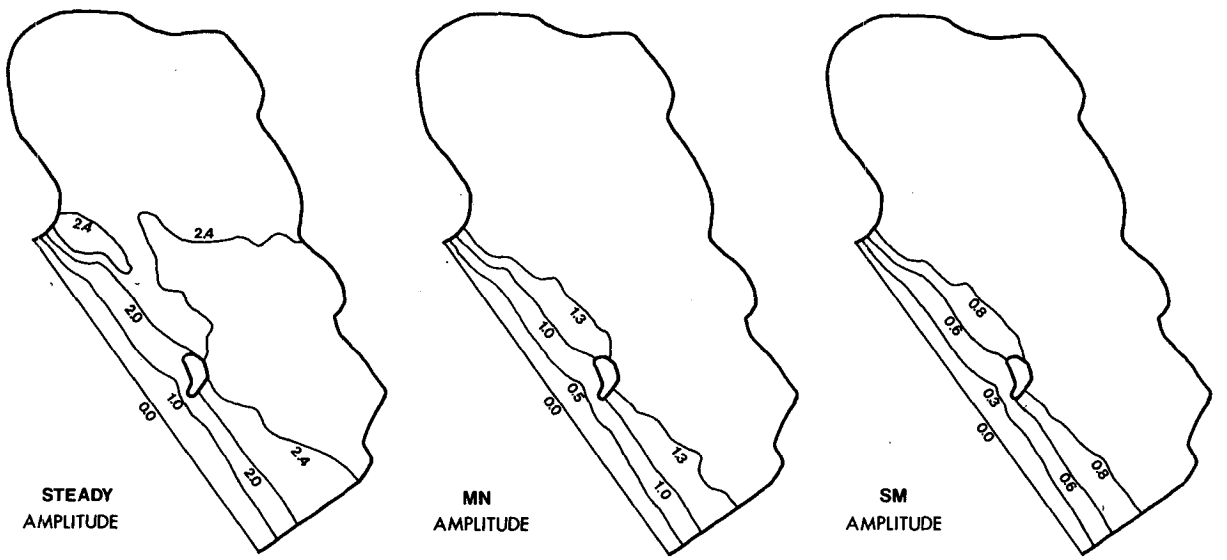

FIG. 6. Computed contours for elevation amplitudes (in cm) for the significant low period constituents for case C-6.

M_4 errors remain at approximately the same level. The errors associated with the additional astronomical constituents are modest, ranging between 16% and 27%.

The addition of the M_2–N_2 compound tides, case C-2, further reduces the M_6 error from 74.7% to 60.5%. We also see a reduction in the N_2 error from 19.6% to 18.5%. As previously discussed, these changes are mainly due to the influence of the $2MN_2$ tide. Although this reduction in N_2 errors seems minor, we note that this is an astronomical constituent being influenced by a compound tide constituent. Other errors are not significantly influenced by the M_2–N_2 compound tides.

Allowing the M_2–S_2 compound tides to interact reduces the M_6 error from 60.5% to 56.4%. Furthermore the S_2 error is reduced from 27.0% to 23.2%. Other constituent errors are not significantly affected. The inclusion of the M_2–N_2–S_2 constituents does not really significantly affect any of the constituent errors. Finally, allowing compound tide constituents involving the O_1 and K_1 constituents to interact further reduces the M_6 error from 55.8% to 51.3%. In addition, the O_1 and K_1 errors see reductions of 1% to 2%, respectively.

These error trends are strictly in accordance with the changes in elevation amplitude discussed in section 5. They substantiate that the trends established in section 5 are in accordance with the field data. These errors again underscore the importance of including the compound tides. In particular, the M_6 error is substantially reduced between case O-4 and case C-5 such that the overprediction has dropped from 99.3% to 51.3% (from a factor of 2.0 to 1.5). This overall error decrease is as much due to the introduction of the secondary astronomical tides (N_2, S_2, O_1 and K_1) as to the interaction of compound tides. In particular the $2MN_2$ and $2MS_2$ constituents significantly influence the M_6 error. Furthermore, the $2MN_2$ and $2MS_2$ constituents influence their associated astronomical constituents.

c. *Re-optimization of c_f with complete compound tide interaction*

In section 6b we examined the elevation amplitude errors associated with varying degrees of astronomical and compound tide interaction using $c_f = 0.0095$. However, this bottom friction value was selected based on being the optimal value for the overtide only cases. Therefore, we now briefly examine whether this value is still optimal when allowing for the more complete nonlinear interactions which include all of the constituents of case C-5.

Prediction errors for various c_f values are shown in Table 12 and indicate that the optimal c_f value (based on the minimum M_2 error only) has shifted to a value of 0.0090. With the exception of the M_6 error all errors benefit slightly from this reduction in friction factor. Table 12 also shows that decreasing c_f below 0.0090 corresponds to a continued downward error trend for the O_1, K_1 and S_2 constituents whereas the N_2, M_2 and M_4 errors all show an upward error trend fairly soon below the optimal value. Thus the final "optimal" value for c_f is selected as 0.0090 corresponding to run C-6. This reduced c_f value is in accordance with Le Provost and Fornerino's (1985) analytical predictions which account for the increased damping effect of the main secondary semidiurnal astronomical constituents.

The final "optimal" prediction errors, S_j^p, obtained for case C-6 are typically significantly larger than the corresponding measurement error, S_j^m, shown in Table

9. We note that to get an estimate of the prediction error which is adjusted for the measurement error, S_j^{p-m}, we must compute the difference in the variances; thus $(S_j^{p-m})^2 = (S_j^p)^2 - (S_j^m)^2$. Therefore, with the exception of the K_1, N_2 and S_2 tides (for which S_j^{p-m} respectively equals 0.11, 0.13 and 0.17), the measurement errors do not significantly affect the prediction error values.

Results for elevation amplitude and phase for significant constituents for this fully compound constituent interacting case C-6 with $c_f = 0.0090$ are plotted in Figs. 5 through 10. Filloux and Snyder's (1979) measured elevation amplitude and phase values, averaged over up to three experiments, are indicated at each measurement site for the M_2, N_2, S_2, O_1, K_1, M_4 and M_6 constituents. Measurement site errors in elevation amplitude are, on average, roughly in accordance with the proportional standard deviations listed in Table 12. Comparing predictions to the average measured values, we note that amplitudes for the M_2 tide are slightly underpredicted in the northern bight, while they are typically somewhat overpredicted in the southern bight. The N_2 elevation amplitudes are under- and overpredicted at roughly an equal number of measurement sites, although in a randomly distributed manner. The O_1, K_1 and S_2 tides are predominantly underpredicted. Overdamped secondary semidiurnal astronomical tides are a commonly encountered prob-

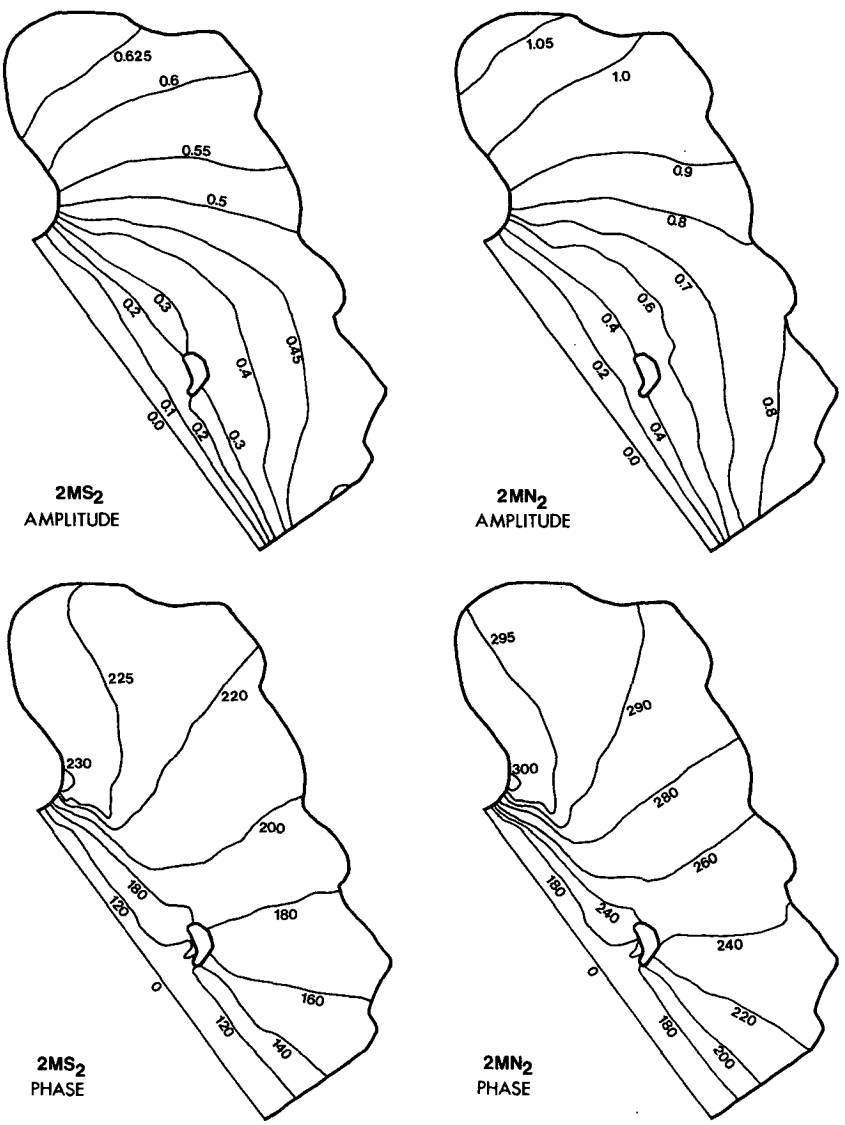

FIG. 7. Computed contours for elevation amplitudes (in cm) and phases (in degrees lag w.r.t. the M_2 constituent at the open ocean boundary) for the significant semidiurnal compound constituents for case C-6.

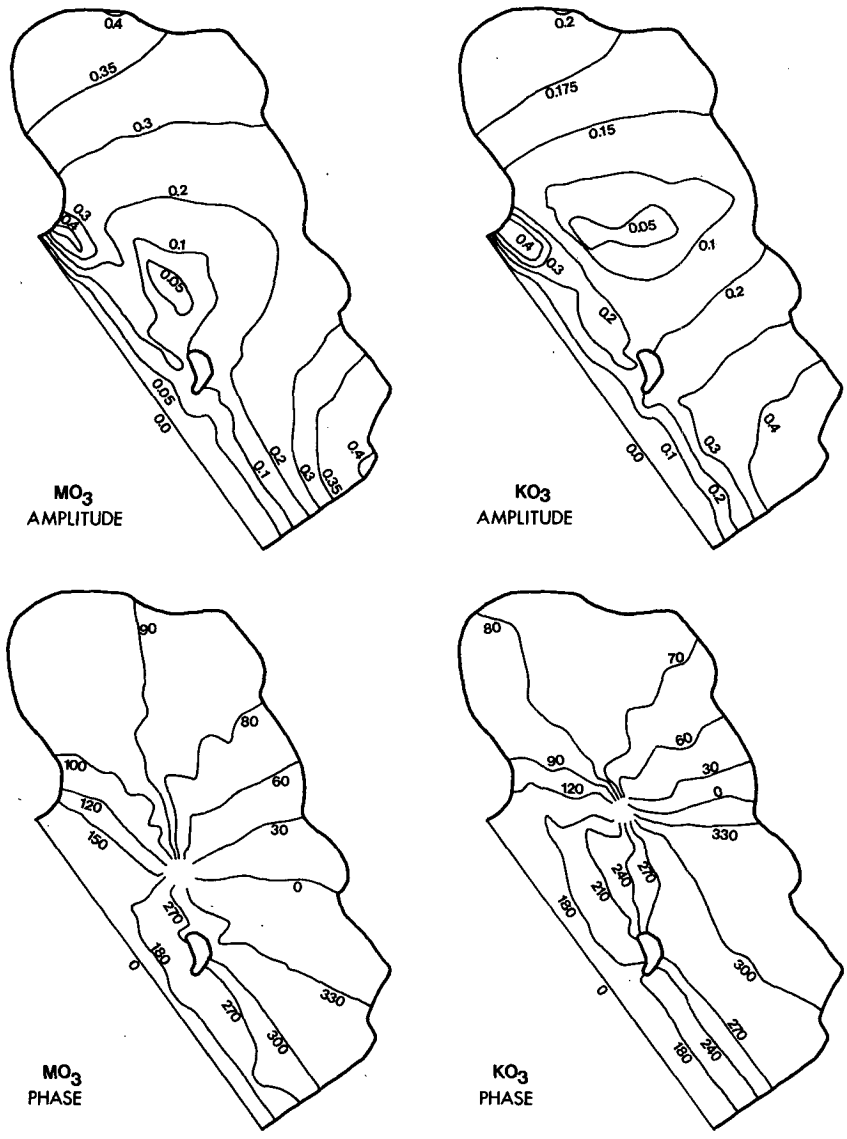

FIG. 8. Computed contours for elevation amplitudes (in cm) and phases (in degrees lag w.r.t. the M_2 constituent at the open ocean boundary) for the significant terdiurnal compound constituents for case C-6.

lem in tidal prediction models (e.g. Le Provost and Fornerino 1985). The M_4 tide is under- and overpredicted at about the same number of sites with discernable regional patterns. The M_6 tide is uniformly substantially overpredicted. We note, in particular, that certain values very near the ocean boundary are underpredicted for both the M_4 and M_6 constituents. This suggests that the application of a fully reflective boundary condition is not entirely correct and causes some portion of the remaining overall errors in the M_4 and M_6 constituents.

Predicted phases, for our optimal run, also compare favorably to the average measured values indicated when taking into account the variability of the measured values. The agreement for the M_2 component is excellent. The N_2, S_2, O_1 and K_1 phase predictions are very good although, in general, slightly overpredicted in the northern bight. The rapidly spatially varying M_4 and M_6 phase predictions also agree very well with the measured values.

The predictions for the astronomical and M_2 overtide constituents are similar in character to those presented by Snyder et al. (1979). However, values and patterns do differ somewhat, in particular for the M_4 and M_6 constituents. We note that Snyder et al. (1979) obtained their optimal solution by allowing for either a significant nontidal current [$O(0.28\ m\ s^{-1})$] or nonquadratic friction law. The solutions we present do not introduce high nontidal currents nor deviate from the standard quadratic friction law. In fact, our optimal solution relies on the inclusion of the interaction of the compound tidal constituents. The M_6 constituent,

in particular, is significantly affected through these interactions.

It is noted that the general structure of both the amplitudes and phases of constituents of the same type and frequency range are extremely similar. Figure 5 indicates that the semidiurnal astronomical constituents, M_2, N_2 and S_2, all show substantial damping and a minimum amplitude point in between the sill and the northern depression region. The diurnal astronomical constituents, O_1 and K_1, are similar to the semidiurnal constituents, although the minimum values have decreased significantly less relative to the corresponding boundary values than is the case for the semidiurnal constituents.

Figure 6 indicates that the low period constituents, steady state, MN and MS, all show sharp gradients in the sill region and little variation elsewhere. This structure results from the finite amplitude terms in both the continuity and momentum equations. For the steady state component, this corresponds to a seaward residual velocity component which balances the net flux to zero along the open ocean boundary.

The relatively strong semidiurnal compound constituents, the $2MN_2$ and $2MS_2$ shown in Fig. 7 have amplitudes which increase steadily towards the northern portion of the bight. The terdiurnal constituents, MO_3 and KO_3 shown in Fig. 8 clearly exhibit amphidromic regions in between the sill and the northern bight region and then steadily increase towards the northern and southeastern shorelines. The quarter-diurnal constituents, M_4, MN_4 and MS_4 shown in Fig. 9, also have an amphidromic region. Finally the sexto-

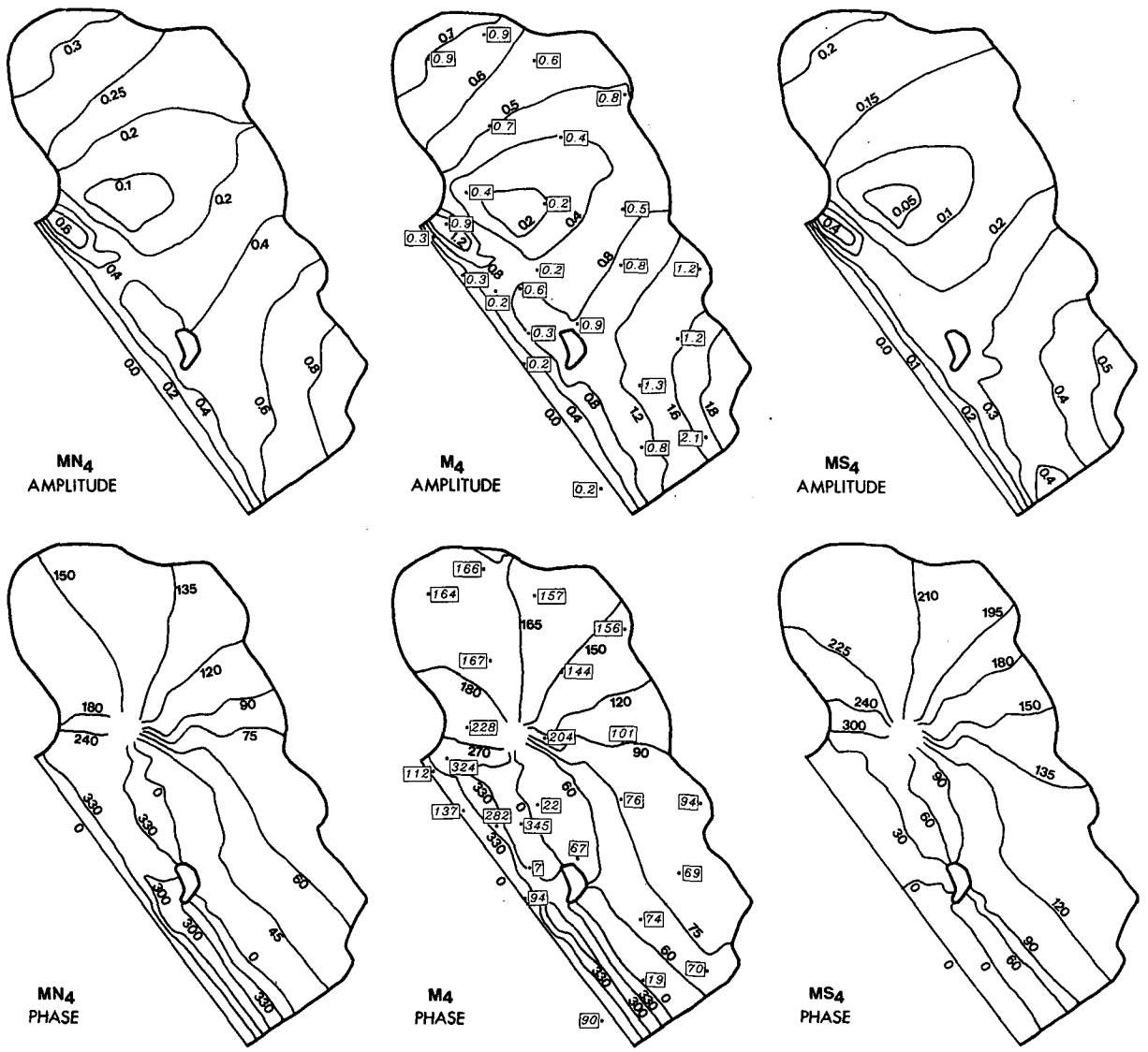

FIG. 9. Computed contours and average measured (boxed) values for elevation amplitudes (in cm) and phases (in degrees lag w.r.t. the M_2 constituent at the open ocean boundary) for the significant quarter-diurnal nonlinear constituents for case C-6.

diurnal constituents, M_6, $2MN_6$ and $2MS_6$ shown in Fig. 10, exhibit an amphidromic region which is located further north than that of other constituents.

7. Conclusions

We have examined the interaction of the various nonlinear terms in the shallow water equations in addition to investigating the influence of the shallow water constituents on each other through the application of model TEA-NL to the Bight of Abaco.

Model TEA-NL's iterative frequency–time domain formulation is ideally suited for this study since this technique allows for the selective suppression of the backfeeding of nonlinear constituents. This allows excellent control over the degree of nonlinear constituent interaction and permits the detailed determination of how the various shallow water constituents affect each other. Time domain models do not have this capability. Furthermore, the tailored least-squares harmonic analysis applied allows for the very efficient resolution and determination of extremely closely spaced and/or long period constituents.

Friction is the single most important nonlinearity in the Bight of Abaco. It dominates the response of the M_2 constituent, which in turn is largely responsible for the generation of the shallow water tides through nonlinear interactions with itself, secondary astronomical constituents, and the shallow water constituents. Furthermore, friction is predominantly responsible for the generation of the important semidiurnal compound ($2MN_2$ and $2MS_2$) and sexto-diurnal compound tides and overtides. Finite amplitude terms in both the continuity and momentum equations are largely responsible for generating low period and the quarter-diurnal

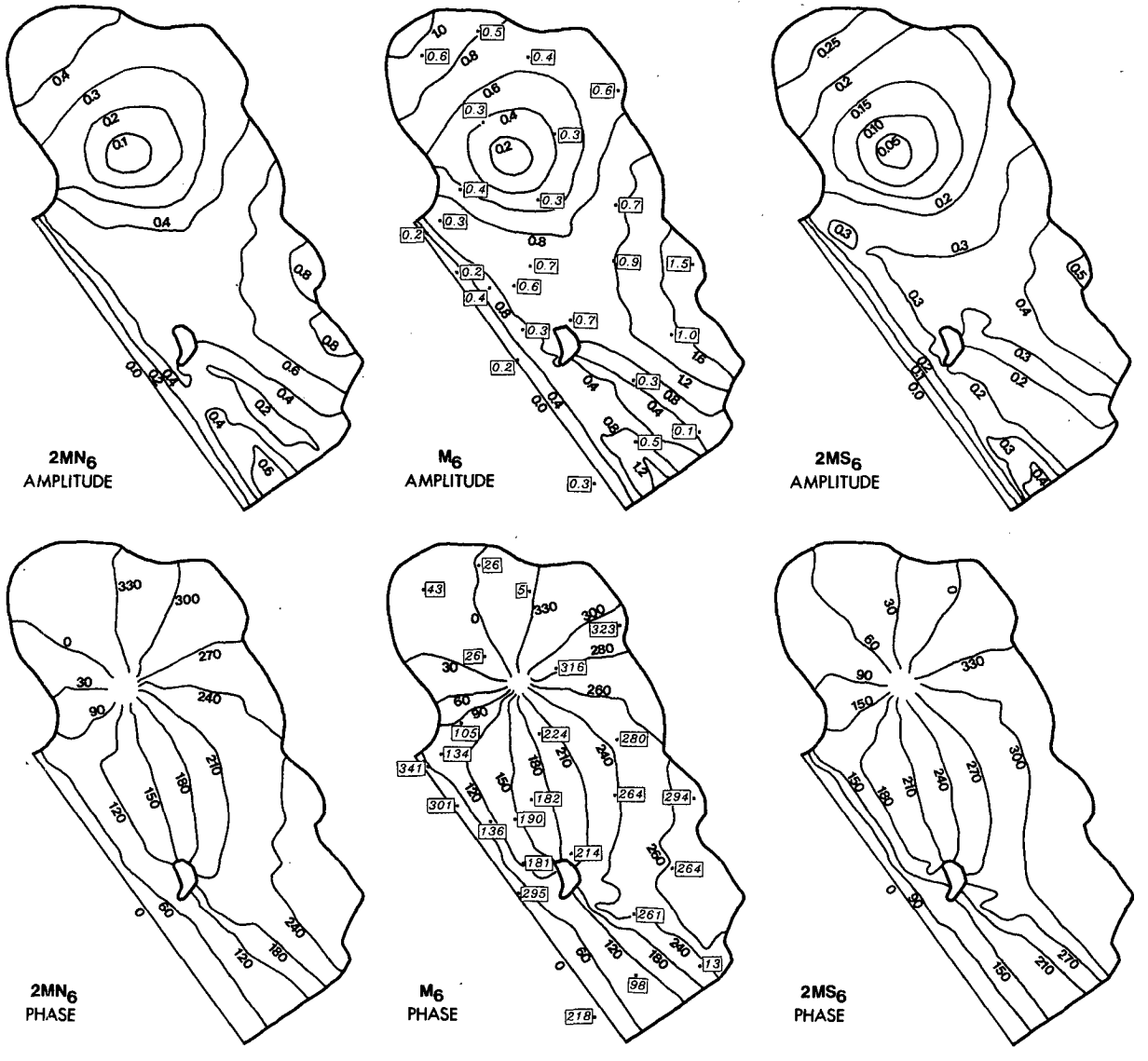

FIG. 10. Computed contours and average measured (boxed) values for elevation amplitudes (in cm) and phases (in degrees lag w.r.t. the M_2 constituent at the open ocean boundary) for the significant sexto-diurnal nonlinear constituents for case C-6.

tides. The combined effect of friction and finite amplitude terms generate the eight-diurnal tides due to the resulting interplay of the sexto-diurnal constituents (generated by friction) and the astronomical constituents through the finite amplitude term. The convective terms do not significantly affect the astronomical tides nor the generation of the nonlinear tides.

A significant aspect of our study is the demonstrated influence that nonlinear constituents have on each other. Nonlinear tides are affected not only by the main M_2 and other astronomical tides but also by the interactions which result between the astronomical and nonlinear tides themselves. Important examples include the dramatic decrease in M_6 response due to the $2MN_2$ and $2MS_2$ constituents and the increase in M_6 response due to the interaction of M_2 with M_{10}. Furthermore, important nonlinear constituents such as the $2MN_2$ and $2MS_2$ can influence secondary astronomical constituents as much as 7%. We further note that compound tides can be important relative to the corresponding adjacent overtides (about half as important) and even relative to adjacent astronomical tides (e.g., $2MN_2$ and $2MS_2$ are about 15% of N_2 and S_2, respectively). Finally, we note that long period tides are generated, which can significantly influence the velocity distribution in the sill region.

The Bight of Abaco simulations we have presented clearly demonstrate the importance of allowing for the full nonlinear interaction of shallow water constituents (particularly $2MN_2$, $2MS_2$, M_4, M_6, M_8, M_{10}). The overprediction problem experienced by Snyder et al. (1979) has been largely resolved simply by including nonlinear shallow water constituents and without using nonstandard friction laws or very high nontidal currents. The correct influence of these interactions is substantiated by Filloux and Snyder's (1979) measurements. However, the M_6 constituent still remains overpredicted by about 50%. Improving the boundary condition specification for all significant nonlinear constituents will certainly improve both the M_4 and M_6 predictions. However, the secondary astronomical constituents are also not entirely satisfactorily predicted. Both the M_6 constituent and the secondary astronomical constituents interact with the M_2 mainly through the nonlinear friction term. We believe that the associated over- and underprediction problems stem largely from the inadequacy of the standard quadratic friction law as suggested by Snyder et al. (1979). The dominant influence of friction in the bight originates in the sill region with large dunes and very shallow depths. The resulting large three-dimensional recirculating wakes behind these dunes brings into doubt the validity of the assumed depth averaged horizontal flow structure and the standard quadratic friction law. The dominant influence of friction on the M_6 constituent and Snyder et al.'s (1979) partial success in reducing M_6 error with a linear/quadratic friction law would certainly support the idea of nonstandard friction laws. Extremely detailed truly 3-D turbulent flow analyses would be required to entirely resolve the question of the friction law. However, the computational capability required for this type of analysis is only presently emerging.

REFERENCES

Dronkers, J. J., 1964: *Tidal Computations in Rivers and Coastal Waters.* Wiley & Sons, 518 pp.

Filloux, J. H., and R. L. Snyder, 1979: A study of tides, setup and bottom friction in a shallow semi-enclosed basin. Part 1: Field experiment and harmonic analysis. *J. Phys. Oceanogr.*, **9**, 158–169.

Godin, G., 1970: The resolution of tidal constituents. *Int. Hydro. Rev.*, **47**, 133–144.

Horn, W., 1959: The harmonic analysis, according to the least squares rule, of tide observations upon which an unknown drift is superposed. *Third Int. Symp. on Earth Tides,* Trieste.

Int. Assoc. Geod., Permanent Commission on Earth Tides.

Ippen, A. T., 1966: *Estuary and Coastline Hydrodynamics,* McGraw-Hill, 744 pp.

Kabbaj, A., and C. Le Provost, 1980: Nonlinear tidal waves in channels: A perturbation method adapted to the importance of quadratic bottom friction. *Tellus,* **32**, 143–163.

Kawahara, M., K. Hasegawa and Y. Kawanago, 1977: Periodic tidal flow analysis by finite element perturbation method. *Comput. Fluids,* **5**, 175–189.

LeBlond, P. H., 1978: On tidal propagation in shallow rivers. *J. Geophys. Res.*, **83**, 4717–4721.

Le Provost, C., and A. Poncet, 1978: Finite element method for spectral modelling of tides. *Int. J. Num. Methods Eng.*, **12**, 853–871.

——, and M. Fornerino, 1985: Tidal spectroscopy of the English Channel with a numerical model. *J. Phys. Oceanogr.*, **15**, 1009–1031.

——, G. Rougier and A. Poncet, 1981: Numerical modeling of the harmonic constituents of the tides, with application to the English Channel. *J. Phys. Oceanogr.*, **11**, 1123–1138.

Lynch, D. R., and F. E. Werner, 1987: Three-dimensional hydrodynamics on finite elements. Part 1: Linearized harmonic model. *Int. J. Num. Meth. Fluids,* **7**, 871–910.

Parker, B. B., 1986: The importance of frictional nonlinear effects on the tidal dynamics of the Deleware River and Bay. *Int. Symp. on Physics of Shallow Bays, Estuaries and Continental Shelves,* Qingdao, People's Republic of China, China Ocean Press.

Pearson, C. E., and D. F. Winter, 1977: On the calculation of tidal currents in homogeneous estuaries. *J. Phys. Oceanogr.*, **7**, 520–531.

Snyder, R. L., M. Sidjabat and J. H. Filloux, 1979: A study of tides, setup and bottom friction in a shallow semi-enclosed basin. Part II: Tidal model and comparison with data. *J. Phys. Oceanogr.*, **9**, 170–188.

Van Ette, A. C. M., and H. J. Schoemaker, 1967: Harmonic analyses of tides—essential features and disturbing influences. *Proc. of the Symposium on Tides,* Monaco. Int. Hydrogr. Bur.

Walters, R. A., 1986: A finite element model for tidal and residual circulation. *Commun. Appl. Numer. Methods,* **2**, 393–398.

——, 1988: A finite element model for tides and currents with field applications. *Commun. Appl. Numer. Methods,* **4**, 401–411.

——, and F. E. Werner, 1988: Experiments on the generation of tidal harmonics. *Proc. Seventh Int. Conf. on Computational Methods in Water Resources,* M. A. Celia et al., Eds., Elsevier.

Westerink, J. J., J. J. Connor and K. D. Stolzenbach, 1987: A primitive pseudo wave equation formulation for solving the harmonic shallow water equations. *Adv. Water Resour.*, **10**, 188–199.

——, ——, and ——, 1988: A frequency-time domain finite element model for tidal circulation based on the least squares harmonic analysis method. *Int. J. Num. Meth. Fluids,* **8**, 813–843.